The effect of high salt intake on RhoA-mDia1 signalling and cytoskeleton in vasopressin neurons

Banruo Li

Department of Physiology

McGill University

Montreal, QC, Canada

December 2022

A thesis submitted to McGill University in partial fulfillment of the requirement of the degree of Master of Science.

Table of Contents

Abstract

High dietary salt (HDS) strongly correlates with cardiovascular diseases and is a major factor contributing to the pathogenesis of hypertension. While the link between HDS and hypertension is well established, the molecular mechanisms underlying HDS-induced increases in blood pressure remain unclear. Recent studies show that HDS leads to neurogenically-mediated increases in sympathetic activity, vascular resistance, and water and sodium retention, revealing a possible involvement of central sodium detection mechanisms in salt-dependent hypertension. Changes in plasma sodium are detected by specialized osmosensory neurons located in the supraoptic and paraventricular nuclei (SON and PVN) releasing vasopressin (VP), antidiuretic hormone causing renal water retention and vasoconstriction, to achieve body fluid homeostasis. Exposing rats to HDS by subjecting them to 7 days of salt-loading via drinking 2% NaCl solution is associated with excessive activation of VP neurons, leading to a VP-mediated increase in blood pressure. The mechanisms underlying excessive VP secretion in HDS are not fully understood. Our previous studies revealed that magnocellular VP neurons harbor unique cytoskeletal networks comprised of a subcortical actin layer, an array of actin comet-like structures, and a somatic scaffold of interweaved microtubules. Notably, VP neuron excitability is proportional to the density of these cytoskeletons. Moreover, 7 days of salt-loading increases the density of actin and microtubule networks in magnocellular VP neurons. Our recent experiments suggest that chronic exposure of rats to mildly elevated sodium chow, which does not elevate blood pressure, also triggers increases in the actin density. Mammalian Diaphanous homolog protein 1 (mDia1) belongs to the Formin family of proteins, as a major direct RhoA effector, it controls actin and microtubule polymerization and stability.

Our data suggest that RhoA and mDia1 are elevated underneath the plasma membrane of VP neurons in the SON and PVN following salt-loading. Indeed, previous studies on non-neuronal cells have demonstrated that RhoA and mDia1 translocate towards the plasma membrane from the cytosol upon activation. Our data indicate that intracerebroventricular (icv) administration of mDia1 inhibitor SMIFH2 decreases actin density in VP neurons. We hypothesize that salt-loading causes an activation of the RhoA-mDia1 pathway to increase the cytoskeletal density and osmosensitivity of magnocellular VP neurons, leading to excessive VP secretion, volume expansion, and contributing to elevated blood pressure and hypertension.

To investigate additional molecular pathways that might be involved in regulating cytoskeletal structures in the SON and their reorganization upon HDS, we used an unbiased approach to analyze the proteome of the rat SON as compared to non-osmosensory brain areas (cortex). Our preliminary mass spectrometry results identified cytoskeleton-related proteins enriched in the SON as compared to the cortex.

Résumé

Le sel alimentaire élevé (HDS) est fortement associé aux maladies cardiovasculaires et est un facteur majeur contribuant à la pathogenèse de l'hypertension. Bien que le lien entre l'HDS et l'hypertension soit bien établi, les mécanismes moléculaires sous-jacents aux augmentations de la pression artérielle induites par l'HDS restent flous. Des études récentes montrent que le HDS entraîne des augmentations à médiation neurogène de l'activité sympathique, de la résistance vasculaire et de la rétention d'eau et de sodium, révélant une implication possible des mécanismes centraux de détection du sodium dans l'hypertension dépendante du sel. Les modifications du sodium plasmatique sont détectées par des neurones osmosensoriels spécialisés situés dans les noyaux supraoptique et paraventriculaire (SON et PVN) libérant de la vasopressine (VP), hormone antidiurétique provoquant une rétention d'eau rénale et une vasoconstriction, pour atteindre l'homéostasie des fluides corporels. L'exposition de rats à l'HDS en les soumettant à 7 jours de charge saline en buvant une solution de NaCl à 2 % est associée à une activation excessive des neurones VP, entraînant une augmentation de la pression artérielle médiée par VP. Les mécanismes sous-jacents à la sécrétion excessive de VP dans le HDS ne sont pas entièrement compris. Nos études précédentes ont révélé que les neurones VP magnocellulaires hébergent des réseaux cytosquelettiques uniques composés d'une couche d'actine sous-corticale, d'un ensemble de structures ressemblant à des comètes d'actine et d'un échafaudage somatique de microtubules entrelacés. Notamment, l'excitabilité des neurones VP est proportionnelle à la densité du cytosquelette. De plus, 7 jours de chargement en sel augmentent la densité des réseaux d'actine et de microtubules dans les neurones VP magnocellulaires. Nos expériences récentes suggèrent que l'exposition chronique des rats à une alimentation en sodium légèrement élevée, qui n'élève pas la pression artérielle, déclenche

également une augmentation de la densité d'actine. Mammalian Diaphanous homolog protein 1 (mDia1) appartient à la famille des protéines Formin, qui, en tant qu'effecteur de RhoA, contrôle la polymérisation et la stabilité de l'actine et des microtubules.

Nos données suggèrent que RhoA et mDia1 sont élevés sous la membrane plasmique des neurones VP dans le SON et le PVN après le chargement en sel. En effet, des études antérieures sur des cellules non neuronales ont démontré que RhoA et mDia1 transloquent vers la membrane plasmique à partir du cytosol lors de l'activation. Nos données indiquent que l'administration intracérébroventriculaire (icv) de l'inhibiteur de mDia1 SMIFH2 diminue la densité d'actine dans les neurones VP. Nous émettons l'hypothèse que la charge en sel provoque une activation de la voie RhoA-mDia1 pour augmenter la densité cytosquelettique et l'osmosensibilité des neurones VP magnocellulaires, entraînant une sécrétion excessive de VP, une expansion du volume et contribuant à une pression artérielle élevée et à l'hypertension.

Pour étudier les voies moléculaires supplémentaires qui pourraient être impliquées dans la régulation des structures cytosquelettiques dans le SON et leur réorganisation on response à HDS, nous avons utilisé une approche impartiale pour analyser le protéome du SON de rat par rapport aux zones cérébrales non osmosensorielles (cortex). Nos résultats préliminaires de spectrométrie de masse ont identifié des protéines liées au cytosquelette enrichies dans le SON par rapport au cortex.

List of figures

Acknowledgments

First, I would like to thank my supervisor Dr. Masha Prager-Khoutorsky for giving me the opportunity to be part of the lab. Thank you for giving me the privilege to work on the amazing neuroscience project at McGill and guide me in every step to not only an independent researcher but also a complete person. She has been the most supportive and caring mentor anyone could have wished for. I would also like to thank my advisory committee members, Drs. Charles Bourque, John Orlowski, and Arnold Ludwig Hayer, for all the helpful insights you kindly provided.

I want to thank all the members in Prager-Khoutorsky's lab, Jieyi, Amirah, Suijian, Ning, Misha, Yining for the warm and supportive environment they create. Especially thank you to Jieyi and Amirah who taught me everything I need in the lab. The endless support from the lab means a lot to me especially under covid situation. Additionally, I want to thank Lorne Taylor and Jennifer Nedow from proteomics platform at Research Institute of the McGill University Health Centre for their help in my mass spectrometry experiments.

Finally, I would not have been capable of accomplishing anything without my family who always love me no matter what: my mom, dad, grandma, and grandpa. And my amazing friends who cheer me up when I feel life is hard: Ayuna who takes care of me as her little sister, Kristina, Yihan, Jiajing.

Contribution of Authors

The experiments were conceptualized and designed by Dr. Masha Prager-Khoutorsky. Banruo Li wrote and completed the following thesis.

Salt-loading

Banruo Li maintained animals during salt-loading, measured daily water consumption and plasma osmolality, performed transcardial perfusion and extracted brains, immunohistochemical experiments, western blotting experiments, confocal and Airy-scan imaging, and collected and analyzed the data.

Icv injection of formin inhibitor SMIFH2

Dr. Ning Gu performed cannula implantation surgery.

Dr. Ning Gu and Banruo Li performed icv injections through implanted cannulas and maintained animals during recovery, SL, and injections.

Banruo Li performed transcardial perfusion and extracted brains, immunohistochemical experiments, and collected, processed, and analyzed the data.

Chronic exposure to elevated sodium chow

Dr. Masha Prager-Khoutorsky maintained animals during the procedure, measured daily water consumption and plasma osmolality, performed transcardial perfusion, and extracted brains.

Banruo Li performed immunohistochemical experiments and collected and analyzed the data.

Mass spectrometry

Banruo Li performed tissue extraction and preparation and analyzed the data.

Proteomics Platform of the McGill University Health Centre (RI-MUHC) performed mass spectrometry processing and protein identification analysis.

Symbols and Abbreviations

+TIPs: plus-end-tracking proteins
AAVs: adeno-associated viruses
ACE: angiotensin converting enzyme
ADH: antidiuretic hormone
AMP: cyclic adenosine monophosphate
Ang II: angiotensin II
APC: adenomatous polyposis coli
ARC: arcuate nucleus
Arp2/3: actin-related protein 2/3
AVP: arginine vasopressin
BDNF: brain-derived neurotrophic factor
BP: blood pressure
CLIP-170: cytoplasmic linker protein 170
CSF: cerebrospinal fluid
CX: cortex
DAD: diaphanous autoregulatory domain
DID: diaphanous inhibitory domain
DRFs: Diaphanous-related formins
EB1: end-binding protein 1
ECF: extracellular fluid
FH1: formin homology 1 domain
FH2: formin homology 2 domain
g: gram
$GABA_AR$: $GABA_A$ receptors
GBD: GTPase binding domain
GPCRs: G-protein-coupled receptors
HC: hippocampus
HDS: high dietary salt
icv: intracerebroventricular
KCC2: K–Cl co-transporter type 2
kg: kilograms
KO: knockout
LARG: leukemia-associated Rho guanine–nucleotide exchange factor
MAPs: microtubule-associated proteins
mDia: mammalian Diaphanous homolog protein
mmHg: millimeters of mercury
MNCs: magnocellular neurosecretory cells
MNPO: median preoptic nucleus

mosmol: milliosmoles
MTs: microtubules
MW: molecular weight
NaCl: sodium chloride
NKCC1: Na–Cl co-transporter type 1
NPFs: nucleation-promoting factors
NSCCs: nonselective cation channels
OT: oxytocin
OVLT: organum vasculosum lamina terminalis
PBS: phosphate buffered saline
PIP2: phosphatidylinositol-4,5-bisphosphate
PKC: protein kinase C
PLC: phospholipase C
PVN: paraventricular nucleus
RAAS: renin-angiotensin-aldosterone system
Rho GAPs: Rho-specific GTPase activating proteins
Rho GEFs: Rho GTPase-specific guanine nucleotide exchange factors
ROCK: Rho-associated coiled-coil forming kinase
SEM: standard error of mean
SFO: subfornical organ
SL: salt-loading
SMIFH2: small molecule inhibitor of formin homology 2 domains
SON: supraoptic nucleus
TrkB: tropomyosin receptor kinase B
V1R: vasopressin 1 Receptor
V2R: vasopressin 2 Receptor
VP: vasopressin
WASP: Wiskott–Aldrich-syndrome protein
ΔN-TRPV1: N-truncated variant of the transient receptor potential vanilloid 1 channel
μm: micrometer

1. Introduction

1.1 Systemic osmoregulation

Osmolality refers to the total concentration of solutes in a solution, expressed in moles per kilogram of solution [1]. Mammals strive to equilibrate the changes between extracellular fluid (ECF) osmolality and cytoplasm osmolality by causing water to flow across cell membranes, which changes cell volume and intracellular ionic strength [1]. Upon large changes in ECF osmolality, cell and tissue integrity can be disrupted by dramatic cell shrinking or swelling. Therefore, mammals maintain the osmolality of the ECF near an osmotic set-point of around 300 milliosmoles per kilogram (mosmol/kg) [1]. For example, humans and rats maintain the ECF osmolality of around 288 mosmol/kg and 294 mosmol/kg, respectively [1]. Failure to properly regulate body-fluid homeostasis can lead to lethal consequences. As it is enclosed in a rigid cranium, the mammalian brain can be damaged by swelling and shrinking. Severe neurological conditions or death can be caused by physical trauma [2,3], and by affected neuronal excitability caused by electrolyte concentration change [4,5].

Although large ECF osmolality changes lead to severe consequences to health, changes in the 1-3% range around the set-point can be compensated by both behavioral and neuroendocrine mechanisms [1]. An increase in ECF osmolality caused by the consumption of salt or the evaporation of water is termed hyperosmolality. It has been established in mammals that hyperosmolality stimulates the sensation of thirst to promote water intake, and also enhances water retention in the kidney mediated by the release of vasopressin (VP). In addition, hyperosmolality increases the rate of natriuresis (sodium excretion) from the kidney, decreases salt appetite, and inhibits panting [1]. In contrast, decreased ECF osmolality resulting from excessive water consumption or insufficient salt ingestion can cause hypo-osmolality. ECF hypo-

osmolality decreases water retention by suppressing basal VP secretion in both rats and humans. Hypo-osmolality can also lead to a reduced sensation of thirst, increased salt appetite, and increased sodium retention [1].

1.2 Vasopressin (VP): antidiuretic hormone

VP, also known as antidiuretic hormone (ADH), arginine vasopressin (AVP), or argipressin, is a small peptidic hormone (MW=1080) synthesized in the somata of hypothalamic magnocellular neurosecretory cells (MNCs) located in the paired hypothalamic supraoptic (SON) and paraventricular nuclei (PVN). VP neurons coexist with MNCs that release oxytocin (OT), a peptide hormone involved in breastfeeding, labor and social bonding [6–8]. MNCs neurons project the axons to the posterior pituitary [9], where the hormones are secreted from the nerve terminals into the circulation (Figure 1). VP secretion is mediated by calcium-dependent exocytosis and is proportional to the rate of the action potentials initiated at MNC somata [10,11].

1.3 VP receptors

VP is irreplaceable in humans. VP deficiency can result in diabetes insipidus (10-15 L of urine per day) [12]. The physiological effects of VP are mediated by binding to three different receptors: vasopressin 1 Receptor a (V1aR), vasopressin 1 Receptor b (V1bR) (also called V3R), and vasopressin 2 Receptor (V2R) [13]. VP receptors are serpentine receptors with seven transmembrane domains coupled to G protein-mediated second messenger pathways [14,15]. V2R activation is mediated by cyclic adenosine monophosphate (AMP), while V1aR and V1bR activation is mediated by calcium signals [16]. Major functions of VP include water reabsorption (antidiuresis) mediated by V2R located on the distal tubules and collecting ducts in the kidney

and vasoconstriction mediated by V1aR located on the vascular smooth muscle cells [16]. But VP receptors are found in many other tissues with different principal effects [17].

1.4 Epidemiology of Hypertension

Hypertension, defined as systolic blood pressure (BP) ≥ 140 mmHg and/or diastolic BP ≥ 90 mmHg, is the leading risk factor for cardiovascular disease worldwide [18,19]. A study in 2016 showed that a total of 1.38 billion people had hypertension in 2010 (31.1% of the global adult population), and this number may reach 1.56 billion by 2025 [20]. The rising prevalence of hypertension worldwide is a result of the aging of the population and unhealthy lifestyles including unhealthy diets (i.e. high sodium and low potassium intake), physical inactivity, and obesity [20]. Although both men and women develop hypertension, world health statistics 2012 stated that males have a higher prevalence of hypertension (29.2%), compared to females (24.8%) [21]. Hypertension affects countries across all income groups but its prevalence is lower in wealthy countries with health awareness [22]. High BP is responsible for around 54% of stroke and 47% of coronary heart disease and accounts for 13.5% of annual mortality worldwide [23].

1.5 Salt-sensitive hypertension

1.5.1 The risk factor of hypertension: excessive sodium intake

As mentioned above, many unhealthy lifestyles account for the prevalence of hypertension. However, it is widely recognized that excessive sodium intake is the most significant risk factor contributing to the development of hypertension [24–27]. Excessive sodium consumption is defined as > 5 g sodium per day by the World Health Organization. However, the estimated dietary salt intake for an adult is about 9-12 g in most countries, which has been suggested to significantly increase BP and be linked to the development of hypertension

and the associated cardiovascular complications [28,29]. A large meta-analysis showed that a reduction in sodium intake from 9-12 to 5-6 g/day for four or more weeks will have a major effect on BP in both hypertensive and normotensive individuals, irrespective of sex and ethnic group, and a further reduction to 3 g/day will cause a greater decrease in BP [30]. Hence, reducing daily salt intake can be a key preventive treatment for hypertension.

1.5.2 Salt-sensitive and salt-resistant

The association between salt intake and BP was first systematically studied by Ambard and Beaujard almost 120 years ago. They noticed that a few patients did not show elevated BP despite massive salt loading [31]. This observation suggests that there is an internal mechanism that regulates arterial pressure. About 40 years later, Dr. Walter Kempner adopted a rigorous salt-deficient rice diet that could decrease the BP significantly of patients with severe hypertension. A cohort of 777 patients treated on the diet for an average of 92 days expressed decreased BP from 196/116 to 150/96 mmHg [32]. Before the advent of antihypertensive drugs, the effects of this radical diet were comparable with an intensive, modern antihypertensive drug therapy [33]. However, only approximately 60% of patients presented a notable decrease in BP following the salt-deficient diet. These patients are known as salt-sensitive. Nevertheless, it took another several decades before the terms salt-sensitive and salt-resistant were extensively used in the literature [34].

People are divided into salt-sensitive and salt-resistant groups based on how their BP levels respond to changes in dietary salt [35,36]. In fact, it is estimated that 50%-60% of hypertensive individuals are salt-sensitive [33]. In addition to the genetic markers that have been found to be associated with salt sensitivity, salt sensitivity is more prevalent in the aging population, Black people, and people with metabolic syndrome or obesity [37,38]. Although the

association between salt-sensitive hypertension and dietary salt intake has been widely demonstrated, concerns have been raised as simply restricting dietary salt intake to control and lower BP has been proved inefficient. This is partly due to a lack of motivation and knowledge to modify and maintain a healthy lifestyle and low-sodium diet [39]. In addition, the fact that people enjoy the flavor of salty food may explain why even a modest reduction in dietary salt is difficult to maintain considering a sodium-rich food environment in post-industrial societies [40,41]. Moreover, long-term restriction of sodium intake is not efficient in controlling BP [42]. Furthermore, the debate has prevailed as to whether a low sodium intake may adversely affect insulin resistance, blood lipids, catecholamines, and cardiovascular disease risk factors [28,43,44]. Finally, a large portion of the salt-sensitive hypertension patients has a resistant type of hypertension which is defined as BP that remains above standard despite the use of three antihypertensive drugs [45,46]. Therefore, elucidation of the pathophysiology of salt-sensitive hypertension will facilitate the development of new therapies to treat patients suffering from resistant hypertension.

1.5.3 Possible mechanisms of salt-sensitive hypertension

Previous studies have reported several possible mechanisms underlying the development of salt-sensitive hypertension. Several of them will be discussed below.

Arterial BP is controlled by both the cardiac output (stroke volume × heart rate) and total peripheral vascular resistance [47]. Based on the fact of influencing these two factors, the following mechanisms have been proposed.

The first mechanism that was proposed is based on its effect on stroke volume thus influencing the cardiac output. As antidiuretic hormone, VP plays an important role in the potential mechanisms [48,49]. Under the basal condition, VP is circulating at a concentration of

0.5-5 pg/ml in humans which is sufficient to regulate body fluid homeostasis by stimulating water retention in the kidney [50]. Previous studies have shown that chronic high dietary salt (HDS) causes an increase in the plasma sodium concentration and blood osmolality, which stimulates an excessive release of VP [51,52]. In fact, studies in rats have shown that high sodium intake can trigger a two-to-three-fold increase in plasma VP [53,54]. As expected, increased plasma VP levels have been observed in other hypertension animal models induced by high salt intake [55–57]. Moreover, studies reported that a plasma VP concentration of 10 pg/ml or higher can cause vasoconstriction via V1R located on vascular smooth muscles [58]. Besides, VP can also stimulate the release of endothelin from endothelial cells that serves as a potent vasoconstrictor. *In vivo* experiments in humans proved that even a small increase in plasma VP level between 0.7 and 6.0 ng/ml caused a significant increase in endothelin production [59]. Therefore, an excessive release of VP into the circulation can promote both water retention and vasoconstriction (Figure 1). Excessive release of VP caused by chronic HDS can induce an accumulation of fluid and blood volume expansion in the vasculature, i.e. hypervolemia (Figure 1) [60]. Hypervolemia can lead to an increase in stroke volume and produces additional pressure on the vasculature, thus contributing to hypertension (Figure 1) [61–65].

An alternative hypothesis was proposed based on the abnormal reaction of the renin-angiotensin-aldosterone system (RAAS) in salt-sensitive hypertension. RAAS is responsible for chronic modifications of blood volume and vascular resistance. This system is mainly composed of three compounds: renin, angiotensin II (AngII), and aldosterone. Under normal physiological conditions, several factors (low sodium intake, arterial pressure decrease, and increased sympathetic activity) can stimulate RAAS. First, the release of renin is increased from the juxtaglomerular cells of the kidneys. Second, renin converts angiotensin I from angiotensinogen,

a peptide hormone synthesized primarily in the liver. Then, Ang II is converted from angiotensin I by the increased release of angiotensin-converting enzyme (ACE) in the lungs. Ang II serves as a potent vasoconstrictor. In addition, it stimulates aldosterone secretion from the adrenal cortex. Aldosterone causes sodium and water reabsorption in the kidney and thus increasing blood volume and BP [66]. Through these mechanisms, RAAS can elevate BP in a chronic manner. It is worth mentioning that ACE is the most common target for antihypertensive drugs [67], as ACE inhibitors can prevent the production of Ang II.

Whereas decreased plasma sodium activates RAAS, increased plasma sodium should suppress RAAS activity and leads to lower circulating concentration of renin, Ang II, and aldosterone. However, this is not the case with salt-sensitive hypertension [68–71]. RAAS escape, defined as a hyperactive RAAS despite the elevated plasma sodium concentration, is suggested due to high levels of renin, Ang II, and aldosterone [72]. RAAS escape may thus contribute to additional sodium and water reabsorption and vasoconstriction and give rise to hypertension.

A third hypothesis involves the failure of baroreceptor inhibition under HDS. Under physiological conditions, when arterial pressure rises, baroreceptors are activated to inhibit the firing of VP MNCs via $GABA_A$ receptors ($GABA_AR$). And the inhibition of VP MNCs activity leads to decreased VP release, thus helping to restore the BP. However, following chronic HDS exposure, this negative feedback mechanism is impaired following an increase in intracellular chloride mediated by a downregulation of the chloride exporter K–Cl co-transporter type 2 (KCC2) expression [73,74]. As a result, $GABA_AR$ mediates excitation instead of inhibition in VP MNCs [73–75], which contributes to the excessive VP release in salt-sensitive hypertension. Choe et al. revealed that KCC2 is downregulated through a brain-derived neurotrophic factor

(BDNF)-dependent activation of Tropomyosin receptor kinase B (TrkB) receptors in the salt-loading hypertension rat model (a well-characterized HDS-induced hypertension rat model referred to as SL) [73], meanwhile upregulation of Na–Cl co-transporter type 1 (NKCC1) has also been shown to contribute to this process in another salt-sensitive hypertension rat model (DOCA-salt hypertension model) [74].

1.6 Regulation of VP release

The main stimulus to trigger the release of VP is increased plasma osmolality. Sodium has a larger influence on VP release than urea or glucose for the same change in osmolality [16]. Other stimuli for VP release include reduction in circulating blood volume and stress [76]. This part of the introduction will mainly focus on the cellular and molecular mechanisms underlying the VP release mediated by the changed plasma osmolality.

As mentioned earlier, VP secretion is proportional to the firing rate of VP MNCs. Previous studies have shown that both extrinsic and intrinsic factors contribute to the firing activity and thus modulate VP secretion [77,78]. Notably, MNCs receive direct excitatory input from the organum vasculosum laminae terminalis (OVLT) [79]. OVLT, as a primary osmosensory area in the brain, harbors a population of intrinsically osmosensitive neurons that project into the SON and regulate VP secretion [79–84]. Moreover, other parts of the nervous system also contribute to the regulations of VP neuron firing, including osmosensory neurons in the subfornical organ (SFO), the median preoptic nucleus (MNPO), and peripheral osmosensory neurons via vagal and spinal pathways [77,78]. Furthermore, previous studies have demonstrated that astrocytes surrounding MNCs inhibit VP MNCs activation by releasing taurine [85,86]. Taurine is a potent agonist of the inhibitory glycine receptors on MNCs [87].

In addition to the extrinsic factors, VP MNCs are intrinsically osmosensitive. Electrophysiological recordings showed that the activity of SON MNCs isolated from adult rodents is increased by hypertonic stimuli and inhibited by hypotonic stimuli without any input from neurons and neighboring glial cells [88–90].

Strikingly, modulation of MNCs' activity in response to osmolality is a mechanical process related to changes in cell volume, namely they are mechanosensitive. Unlike many other cell types, which adopt compensatory mechanisms to partly or completely resist cell volume changes elicited by osmotic changes [91,92], MNCs exhibit changes in cell volume that are inversely proportional to ECF osmolality [90,93]. Importantly, these changes can be sustained for many minutes and hours, as MNCs should remain active to secrete VP in order to promote water retention in the kidney before the plasma osmolality returns to the set point [94]. Cell shrinkage induced by hypertonicity causes an increase in the firing rate of these neurons, whereas cell swelling induced by hypotonicity inhibits the basal activity of MNCs neurons (Figure 2). Moreover, the regulation of MNCs activity is dependent on a mechanical effect directly linked to changes in cell volume, but not on changes in ionic strength or solute concentration [90]. Indeed, cell shrinkage or swelling by increasing or decreasing the pressure inside a recording patch pipette can cause quantitatively equivalent changes in MNCs activity as those caused by osmotic stimulation [95]. Likewise, the osmolality-induced changes in MNCs activity can be reversed by regulating cell volume via applying increasing or decreasing pressure through a recording pipette [95].

The intrinsic osmosensitivity of MNCs is mediated by the activation of nonselective cation channels (NSCCs). Recent reports have demonstrated that this channel is encoded as a truncated N-terminal variant of the transient receptor potential vanilloid 1 channel (ΔN-TRPV1),

but not the full-length product (known also as the capsaicin receptor) [96,97]. Mice lacking the expression of the Trpv1 gene show chronically increased plasma osmolality and attenuated VP activity to hypertonic stimulation *in vivo* [83,96]. Furthermore, MNCs acutely isolated from Trpv1 knockout mice lack intrinsic osmosensitivity as they do not respond to neither hypertonic stimuli nor mechanical stimuli that induce shrinking [83,96]. Additionally, the expression of ΔN-TRPV1 restores neuronal responses to hypertonicity and suction applied through a recording pipette in cultured hypothalamic neurons from Trpv1 knockout mice or in a heterologous cell line [97]. Therefore, ΔN-TRPV1 serves as a mechanosensitive ion channel that mediates the MNCs' activation and inhibition triggered by osmotic or mechanical stimuli.

Recent studies have shown that specialized cytoskeletal structures are involved in the mechanical regulation of MNCs by ΔN-TRPV1. In the next section, two elements of the cytoskeleton will be discussed in detail.

Recent studies have demonstrated that the intrinsic osmosensitivity of MNCs is dependent on a unique cytoskeletal network comprised of a subcortical actin layer, an array of actin comet-like structures, and a somatic scaffold of interweaved microtubules.

1.6.1 The role of actin

Acutely isolated MNCs from the rat SON feature a thin layer of actin filaments located underneath the plasma membrane (Figure 3) [98,99]. Studies have shown that this actin layer is involved in the activation of MNCs in response to osmotic stimuli. Disruption of actin filaments with cytochalasin D decreases the density of the actin layer and attenuates cell activation in response to both hypertonic stimulus and suction (Figure 3). In contrast, cell activation is enhanced upon stabilizing the actin network in acutely isolated MNCs with jasplakinolide (Figure 3) [98].

Additionally, the osmosensitivity of VP MNCs is enhanced by Ang II in an actin-dependent manner. Evidence has suggested that Ang II can potentially be released from the SFO to increase VP release during hypovolemia [100,101] or hypotension [102]. Furthermore, the effect of Ang II is mediated by a signaling pathway that includes phospholipase C (PLC) and a calcium-dependent form of protein kinase C (PKC), which also causes a rapid increase in cortical actin density in acutely isolated MNCs [99]. Indeed, studies in isolated MNCs showed that depolymerization of the actin cytoskeleton with cytochalasin D abolishes the effect of Ang II on the enhancement of mechanosensitivity, whereas stabilization of the actin cytoskeleton with jasplakinolide enhances the mechanosensitivity itself and occludes the effect of Ang II [99]. Thus, these findings suggest that the presence of an intact subcortical actin layer is essential for the intrinsic mechanosensitivity of MNCs.

Additionally, actin organization in MNCs has been characterized *in situ* in rats using super-resolution imaging with AiryScan confocal microscopy analysis (Figure 5) [103]. In addition to the subcortical actin layer observed in isolated MNCs, MNCs in the SON and PVN also feature a cytoplasmic array of comet-like actin structures (Figure 5). Moreover, SL dramatically increases the density of subcortical and cytoplasmic actin networks (Figure 5). These results suggest that the increased osmosensitivity of VP neurons under chronic exposure to HDS might be mediated by the reorganization of actin structures in VP MNCs. Previous studies have indicated that actin does not bind directly to TRPV1 channels [104,105], which suggests that actin may not directly regulate the VP MNCs' activity via ΔN-TRPV1. The mechanism by which actin regulates VP neuron activation is pending further exploration.

1.6.2 The role of microtubules (MTs)

Microtubules (MTs), as the most rigid cytoskeletal filaments in the cell, also contribute to the regulation of VP MNCs' osmosensitivity. *In situ* studies have shown that VP MNCs in the SON and PVN exhibit a scaffold of interweaved MTs that occupies the entire cytosol of the cell body [106]. Moreover, this MT scaffold extends all the way to the plasma membrane, with MT tips approach and contact the plasma membrane. This exceptionally complex and dense MT network is strikingly different from MT structures in other neurons (e.g., hippocampus, cortex, cerebellum). However, a similar MT network is also found in OVLT osmosensory neurons. Thus, this MT structure may be a unique feature of hypothalamic osmosensory neurons.

Studies on acutely isolated MNCs revealed that MTs contribute to the osmotically and mechanically induced activation. MNCs' responses to hypertonicity or suction can be abolished by nocodazole which disrupts MT polymerization and is enhanced by MT-stabilizing drug taxol (Figure 3) [106]. Additionally, MT density significantly increases upon SL in VP MNCs of the SON and PVN while MT density in other brain regions remains unchanged (Figure 4) [107]. These results imply that MT structures play an important role in MNCs activation in response to osmotic stimuli, and possibly contribute to the excessive release of VP and elevated BP during salt-sensitive hypertension such as SL.

As mentioned earlier, MT tips interact with the plasma membrane, where ΔN-TRPV1 channels are located. Indeed, immunoprecipitation experiments and *in situ* proximity ligation assay proved that MTs interact with ΔN-TRPV1 channels directly in MNCs [106]. This is supported by the fact that both monomeric tubulin and polymerized MTs can directly interact with TRPV1 channels *in vitro* via two highly conserved tubulin-binding domains on the C-

terminus [108,109]. Moreover, disruption of MT-TRPV1 interaction abolishes neuronal activation induced by mechanical stimuli.

Interestingly, disrupting the tubulin-TRPV1 interactions diminishes suction-induced neuronal activation, but does not prevent the effect of Ang II, a neuropeptide that can activate TRPV1 channels directly in the SON neurons [106]. In addition, increasing or decreasing the number of MT-TRPV1 interaction sites at the surface of MNCs by nocodazole and taxol can proportionally affect the mechanosensitivity of MNCs. These results support the idea that mechanical activation of ΔN-TRPV1 channels requires physical interaction with MTs, whereas ΔN-TRPV1 channels themselves remain functional for other types of non-mechanical stimuli such as an application of Ang II.

Based on these findings, a "push-activation model" has been proposed to explain the MT-TRPV1 interactions required by mechanical activation of MNCs [106]. The "push-activation model" suggests that MTs are connected to ΔN-TRPV1 on the cell surface under the basal condition. Following osmotically-mediated cell shrinkage, the plasma membrane moves inward and compresses the MT network underneath. As a result, compressed MTs exert a pushing force on ΔN-TRPV1 channels on the cell surface, leading to the activation of ion channel ΔN-TRPV1. This model is supported by the rapid kinetics (4 milliseconds) of channel activation by mechanical stimuli measured using single-channel cell-attached recordings. Further studies are required to test the push-activation model and evaluate whether cell shrinkage leads to the compression of MT and subsequent activation of ΔN-TRPV1 channels.

1.7 Mechanisms involved in cytoskeleton regulation

Animal cells depend on protein polymers to form a versatile cytoskeleton that helps to establish cellular shapes, maintain mechanical integrity and motility and is involved in processes

including endocytosis, cell division, force transmission, adhesion, and intracellular transport. These functions are supported by three cytoskeletal filament types: actin, microtubules, and intermediate filaments.

1.7.1 Actin structure and regulation

In animal cells, actin presents in two distinct states: the monomeric globular G-actin and filamentous actin filaments. In contrast to intermediate filaments and microtubules, actin filaments are considered the most dynamic cytoskeleton structure which can mediate drastic structural changes. The balance of G-actin and actin filaments underlies the dynamic modulation of the actin cytoskeleton [110]. G-actin can polymerize to right-handed helical actin filaments, with a typical length of up to 6-7 μm in *in vitro* studies [111]. The rate-limiting step of actin polymerization *in vitro* is the initial step of actin filament formation, known as nucleation [112]. During the nucleation process *in vitro*, actin monomers assemble to generate a dimer and a trimer, which are known as nucleation seeds. The subsequent addition of actin monomers to the nucleation seeds is energetically favorable thus resulting in rapid filament elongation [113]. Actin filaments are polarised, with the slow-growing end termed pointed or minus end and the fast-growing end termed barbed or plus end. The plus end can have a ten times higher polymerization rate than the minus end [113]. As actin is an ATPase, the plus end contains more ATP-bound actin while the minus end contains more ADP-bound actin.

A large number of regulatory proteins in cells can bind to and regulate G-actin and actin filaments, contributing to the formation and dynamics of a range of macromolecular structures, such as lamellipodia, filopodia, stress fibers, and actin cortex [110]. Among those regulatory proteins, three major categories of actin nucleation factors have been discovered: the actin-related protein 2/3 (Arp2/3) complex together with its nucleation-promoting factors (NPFs) and

proteins of the Wiskott–Aldrich syndrome protein (WASP) family, formins, and tandem-monomer-binding nucleators [114].

The Arp2/3 complex can generate branched actin filaments by promoting actin nucleation after binding to the side of an existing filament in the presence of NPFs *in vitro*, which plays an important role in the formation of lamellipodium [110]. The formin proteins have been shown to generate unbranched actin filaments by nucleating actin independently of the Arp2/3 complex [115,116].

1.7.2 A general review of formins

Among many MT nucleators that have been identified, such as gamma-tubulin, microtubule-associated proteins (MAPs) [117], and MT stabilizers such as formins, formin proteins can simultaneously regulate actin and MTs [118].

Formins are a large class of actin-associated proteins that is evolutionarily conserved [118–120]. Key functions of formin proteins include nucleation, actin filament elongation via profilin [121–123], actin filament bundling [124–126], and MT stabilization. Formins appear to stabilize MTs through not only direct binding [127,128], but also via indirect regulation by the MT plus-end tracking proteins (+TIPs) such as adenomatous polyposis coli (APC) and end-binding protein 1 (EB1) [128,129], and by altering the post-translational state of MTs [130]. There are 15 mammalian formins that have been identified. The largest subset is called the Diaphanous-related formins (DRFs). DRFs encompass four mammalian families: mDia, Daam, FMNL, and FHOD, sharing a similar domain organization (Figure 6) [131]. DRFs are composed of an N-terminal GTPase binding domain (GBD), diaphanous inhibitory domain (DID), a C-terminal formin homology 1 and 2 domains (FH1 and FH2 respectively), and a diaphanous autoregulatory domain (DAD) [132–136]. DRFs are in an autoinhibited state through DID-DAD

interactions (Figure 6). Recent studies have shown that the N-terminus physically prevents the function of the C-terminus to promote actin and MT polymerization [136–138]. Autoinhibition through DID-DAD interactions can be released by Rho-GTPase binding to GBD, which allows the active conformation to take place (Figure 6). The catalytic domains FH1 and FH2 can be exposed. The FH1 domain that contains proline-rich motifs can interact with the profilin-actin complex, thereby recruiting G-actin, while the FH2 domain forms a ring-shaped anti-parallel dimer that can mediate actin nucleation and filaments elongation at the plus end [118].

1.7.3 Coordination of actin and MT cytoskeleton by mammalian Diaphanous homolog protein 1 (mDia1)

mDia1 (also known as DIAPH1 or DIAP1) is a member of the DRFs and has been identified as a downstream effector of the small GTPase RhoA, controlling the formation of actin stress fibers [139]. As mentioned earlier, mDia1 is activated when Rho-GTPase binds to the GBD.

Small GTPases of the Rho family play a major role in the reorganization of the actin cytoskeleton. Studies have shown that Cdc42 and Rac can regulate the formation of filopodia and lamellipodia respectively [140–142]. As the effectors of the above GTPases, Wiskott–Aldrich-syndrome protein (WASP) and N-WASP induce actin nucleation by interacting with the Arp2/3 complex [143,144]. While Rho mainly mediates the formation of focal adhesions and stress fibers [145]. The Rho subgroup of the Rho family of GTPases consisting of RhoA, RhoB, and RhoC, serves as a molecular switch in cellular processes such as cell migration, adhesion, morphogenesis, and cytokinesis [146,147]. The conversion of Rho from the GDP-bound inactive form to the GTP-bound active form is catalyzed by the DbI family of Rho GTPase-specific guanine nucleotide exchange factors (Rho GEFs) [148], whereas the conversion from the GTP-

bound form to the GDP-bound form is mediated by intrinsic GTPase activity stimulated by Rho-specific GTPase activating proteins (Rho GAPs) [149]. There are two major effectors of Rho: mDia1, which contributes to the nucleation and actin filaments polymerization, and Rho-associated coiled-coil forming kinase (ROCK), which can activate myosin to bundle actin filaments and cluster extracellular-matrix-ligated integrins, forming stress fibers and focal adhesions [150].

mDia1 plays an important role in actin nucleation and unbranched actin filament elongation as highlighted above, contributing to the formation of various actin-based cellular structures and mediating cellular functions such as cell migration, cell polarization, endocrine trafficking, exocrine vesicle secretion, and phagocytosis [131]. mDia1 has also been suggested to serve as a mechanosensitive regulator of actin polymerization using kinetic models [151,152]. Furthermore, mDia1 has been shown to bind to MTs directly [153], inducing MT stabilization. MT plus-end-tracking proteins EB1 and APC are detected with mDia1 at stable MT ends, potentially indicating that they form a capture complex to stabilize MT tips [154]. Moreover, another MT plus-end-tracking protein cytoplasmic linker protein 170 (CLIP-170) was found to directly interact with the FH2 domain of mDia1 [155]. Previous literature has shown that MT stabilization is mediated by the FH2 domain of mDia, which also mediates actin nucleation and actin filaments elongation [129,156]. *In vitro* studies in HeLa cells indicated that mDia1 may coordinate MTs and actin filaments through its FH2 and FH1 regions, respectively [157]. Moreover, although mDia1 binds to MTs in the presence of actin monomers, the actin polymerization activities mediated by mDia1 can be partially inhibited by the presence of MTs [153]. RNAi approaches have implied that mDia1 is essential for stabilizing MTs in a variety of

different cell types, including fibroblasts [158,159], glioma cells [160], and endodermal cells [161].

Previous work on non-neuronal cells has demonstrated that active mDia1 can be recruited to the plasma membrane [162–164]. Indeed, it is well established that RhoA translocates from the cytosol to the plasma membrane following activation in mammalian cells [165]. The molecular mechanism underlying the translocation of mDia1 upon activation is not fully understood. However, formin translocation from cytoplasm to plasma membrane following activation has been reported in several studies [131,163,166,167]. Within mDia family, mDia1 and mDia2 but not mDia3, comprise a membrane-binding motif composed of polybasic clusters N-terminal to the GBD, which potentially mediates the interaction with phospholipids through electrostatic interactions [164]. The authors proposed a putative mechanism by which active RhoA recruits mDia1 to the plasma membrane, leading to the binding of mDia1 to the plasma membrane by the N-terminal region, and subsequently the clustering of phosphatidylinositol-4,5-bisphosphate (PIP_2) to anchor mDia1 to the plasma membrane in the C-terminus. In this thesis, RhoA and mDia1 localization in VP neurons will be further examined.

1.7.4 Formins in neurons

Coordination from both actin and MT cytoskeletons contributes to the morphological complexity and intracellular compartmentalization of neural cells and mediates almost all critical physiological processes in neurons. The roles of formins in neural functions have been extensively studied. Formins have been suggested to be involved in a variety of neurological disorders: Charcot-Marie-Tooth disease [168–170], non-syndromic intellectual disability [171,172], oligopathies [173], and microcephaly [174], amyotrophic lateral sclerosis [175], schizophrenia [176,177], and obsessive-compulsive disorder [178]. However, the causal

relationship between impairments in Formin functions and these disorders is yet to be established.

mDia1 has been suggested to regulate various stages of neuronal dynamics. Microcephaly has been reported in three unrelated families who carry the homozygous loss of mDia1 [174,179], which is consistent with the fact that all mDia subfamilies contribute to cell division [180]. However, this finding in humans is inconsistent with the double knockout of mDia1 and mDia3 in a mouse model that shows no microcephaly [181]. On the contrary, double knockout of both mDia1 and mDia3 in mice impairs the integrity of the apical adherens junctions and the development of neuroepithelial polarity [181]. In addition, mice lacking mDia1 and mDia3 show a deficiency in tangential migration of cortical inhibitory interneuron precursors, which is mediated by the disruption of actin filaments but not MTs [182].

There is a mutual regulation of actin and MT stability in axons, which makes mDia1 an attractive candidate for axonogenesis. Double knockout of both mDia1 and mDia3 in mice causes aberrant axon crossing of corticospinal neurons and spinal cord interneurons [183]. Additionally, mDia1 can facilitate the growth in response to a neural chemokine, stromal cell–derived factor (SDF)-1α in cerebellar granule cells [184] and entorhinal cortical neurons [185]. Moreover, a recent study has suggested that mDia1 contributes to the maintenance of axon initial segment composition and length, which is mainly mediated by MTs but partially by actin [186].

Moreover, mDia1 has also been shown to be involved in dendritic regulation via the regulation of Golgi movement into dendrites [187]. mDia1 was found to be essential for RhoA-dependent dendritic Golgi polarization and dendritic growth in hippocampal neurons. This result is consistent with previous research in non-neuronal cells showing that RhoA-mDia1 is also required for actin-dependent Golgi dispersion in Hela JW cells [188]. The observed

morphological phenotype is similar to what was reported in another study which suggests that knockdown of mDia1 leads to increased MT catastrophe frequencies in hippocampal neurons [189]. However, whether this mDia1-dependent dendritic regulation is mediated by MTs needs further confirmation.

In this thesis, the expression and roles of mDia1 in VP MNCs will be further studied.

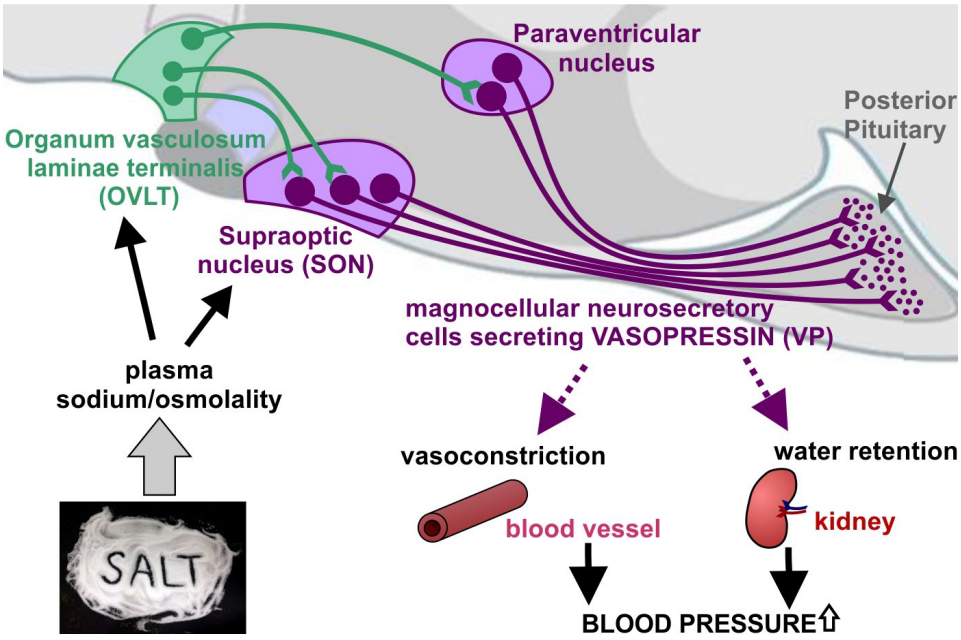

Figure 1. Central osmoregulatory circuits contribute to the increase in blood pressure (BP). HDS consumption increases plasma sodium/osmolality, contributing to the activation of magnocellular VP neurons in the SON and PVN. Activation of VP neurons triggers VP release from the posterior pituitary into the peripheral circulation, leading to vasoconstriction and water retention in the kidney, resulting in an increase in blood volume, peripheral resistance, and contributing to elevated BP (Adopted from Prager-Khoutorsky et al., *Curr Hypertens Rep*., 2017).

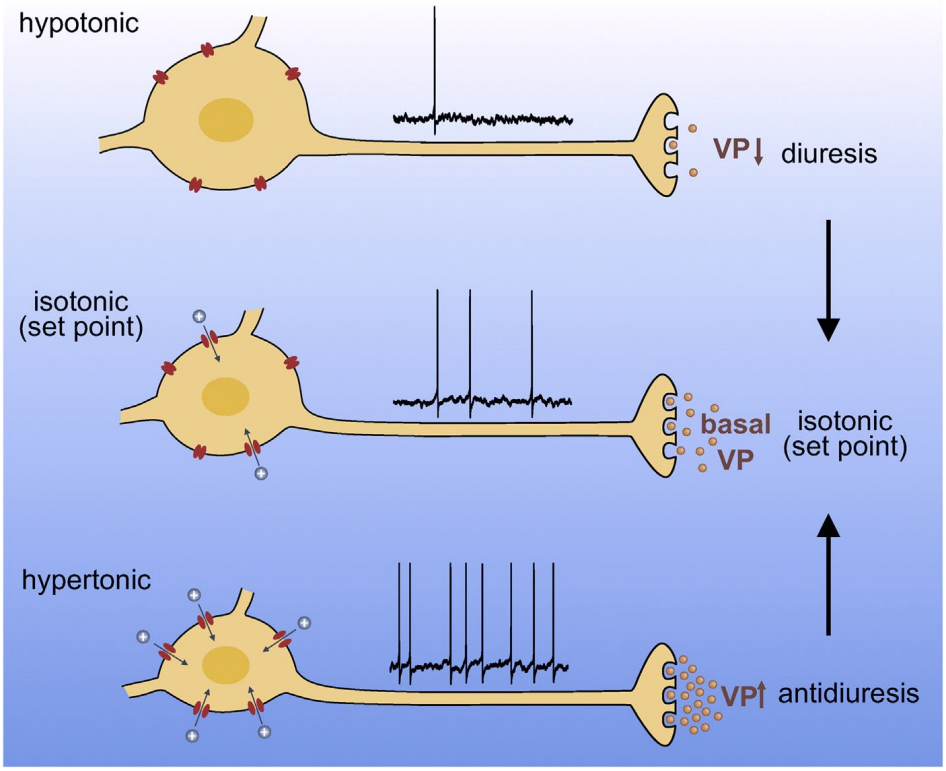

Figure 2. Intrinsic osmosensitivity of VP neurons.
The cell volume of VP neurons can be reversibly changed by plasma osmolality. Hypertonicity-evoked shrinkage activates ΔN-TRPV1 opening, leading to depolarization, an increase in the firing rate, and more VP release. Elevated VP levels in the circulation enhance water absorption by the kidney (antidiuresis) to restore body fluid homeostasis. Hypotonicity induces swelling and inhibits ΔN-TRPV1 that are open under basal isotonic conditions, resulting in hyperpolarization, a decrease in the firing rate, a reduction in VP release, and following diuresis (Adopted from Prager-Khoutorsky, *Semin Cell Dev Biol*, 2017).

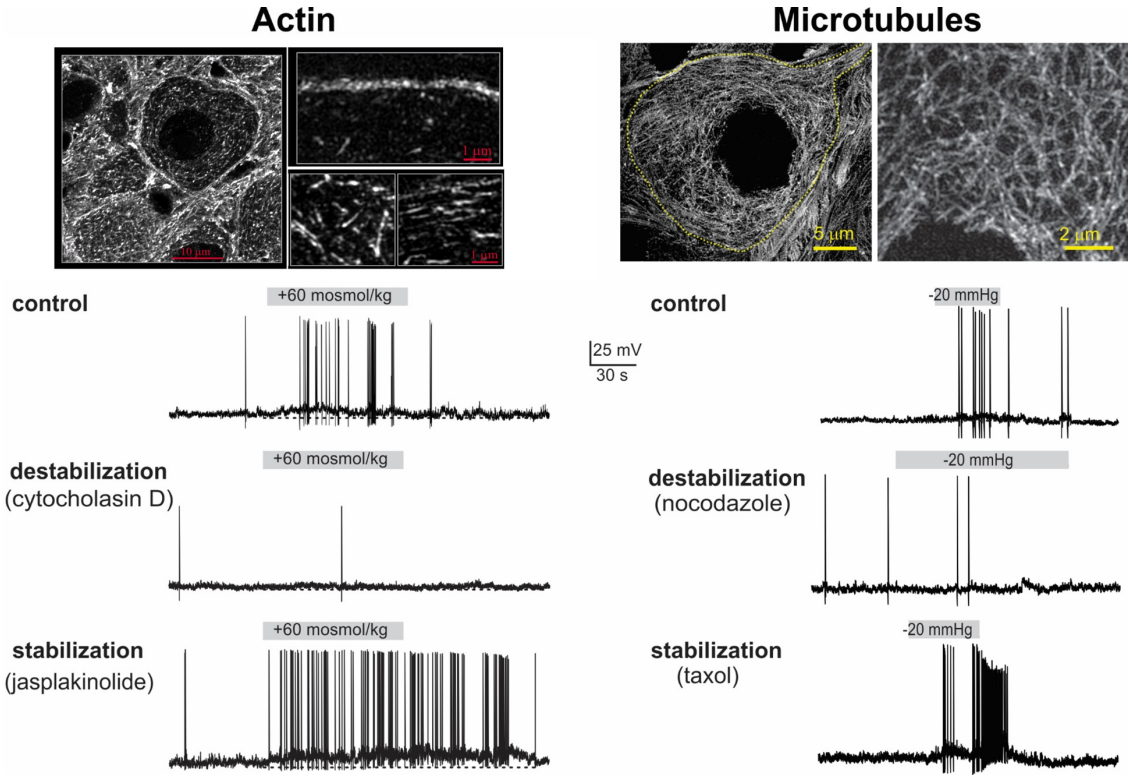

Figure 3. Intrinsic osmosensitivity of VP neurons is regulated by actin and MTs.
VP neurons are comprised of a subcortical actin layer, an array of actin comet-like structures, and a somatic scaffold of interweaved MTs. Studies on isolated rat SON VP neurons have shown that modulating the stability of actin and MTs with pharmacological approaches (stabilizing agents: jasplakinolide and taxol; destabilizing agents: cytochalasin D and nocodazole) can affect the sensitivity of neuronal activation (Adopted from Zhang and Bourque, *J. Neurosci*, 2008, Prager-Khoutorsky et al., *Neuron*, 2014, Barad et al., *eNeuro*, 2020, and Prager-Khoutorsky, *Semin Cell Dev Biol*, 2017).

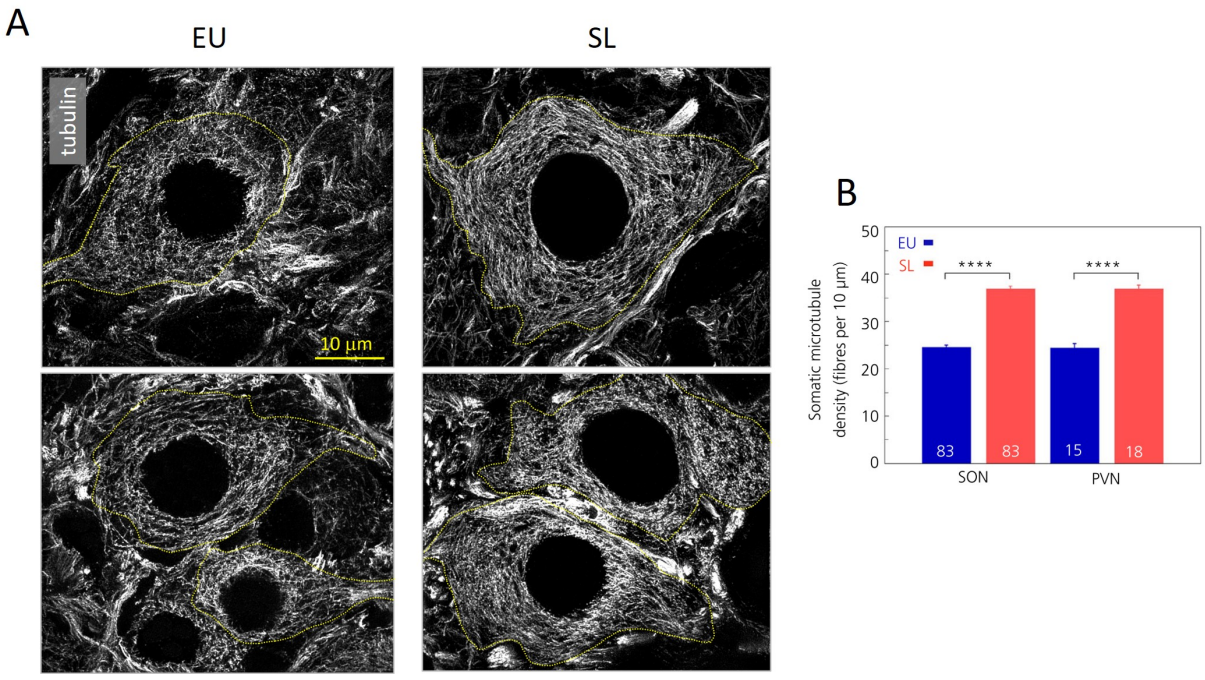

Figure 4. Increased MT density in VP neurons following SL.
A) Immunostaining for α-tubulin (white) in magnocellular VP neurons from euhydrated (EU) and SL rats. **B)** VP neurons exhibit increased somatic MT density in the rat SON and PVN following SL. SL (n = 7); EU (n = 8). Data are reported as mean ± SEM. (****$p < 0.0001$). (Adopted from Hicks et al., *J. Neurosci*, 2020).

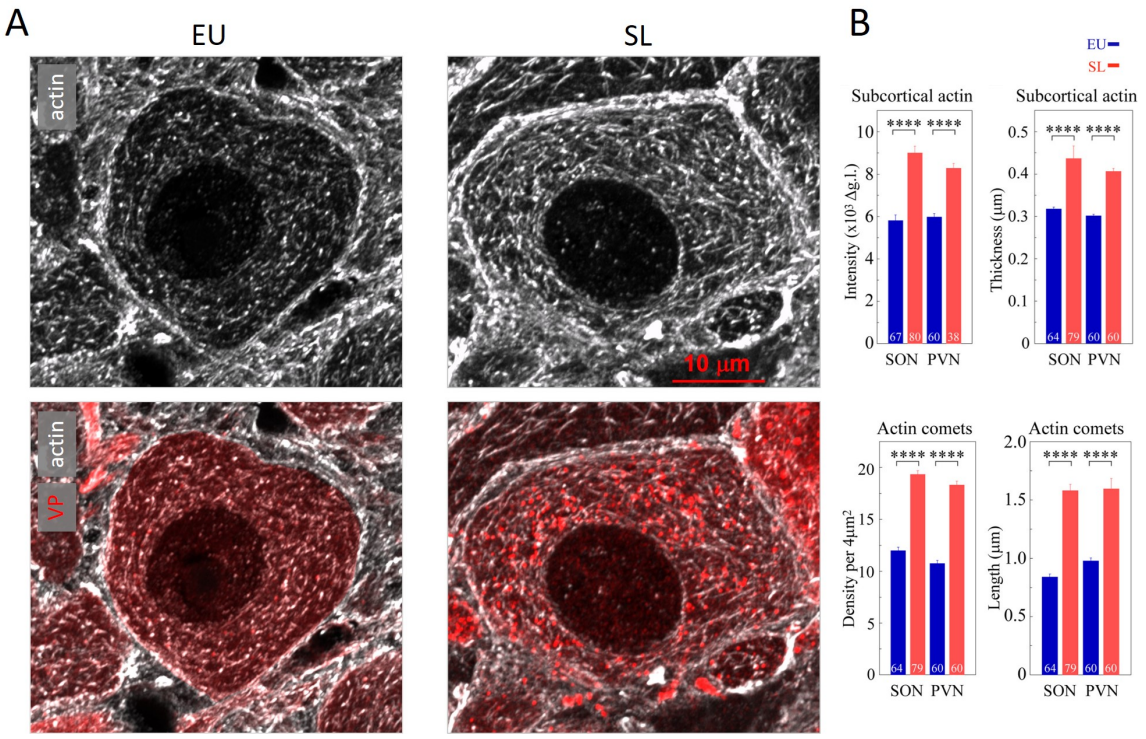

Figure 5. Increased actin density in VP neurons following SL.
A) Immunostaining of β-actin (white) and VP (red) in magnocellular VP neurons from euhydrated (EU) and SL rats. **B)** Subcortical actin intensity and thickness, and comet-like actin structure density and length are increased significantly in the rat SON and PVN following SL. SL (n = 7); EU (n = 8). Data are reported as mean ± SEM. (****p < 0.0001). (Adopted from Barad et al., *eNeuro*, 2020).

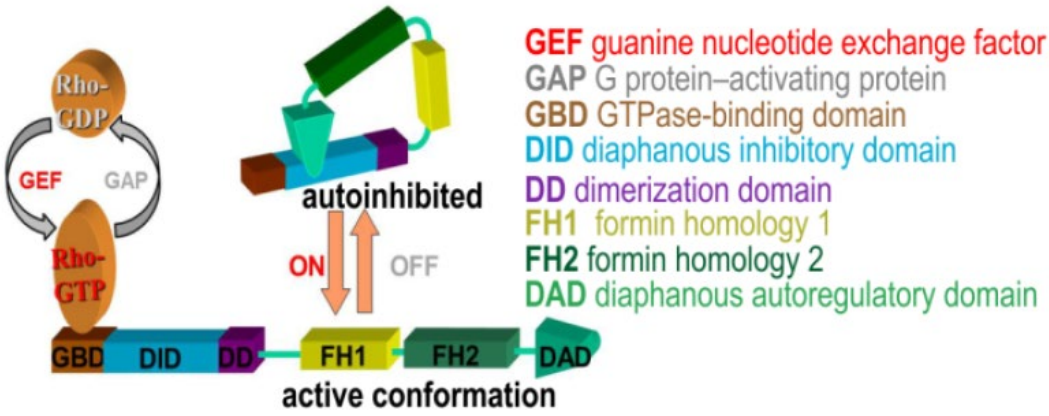

Figure 6 Structure and conformation of Diaphanous-related formins (DRFs).
At the baseline non-activated confirmation, DRFs are folded in an autoinhibitory state caused by intramolecular interactions between the DAD domain and DID domain. The binding of Rho GTPases can release autoinhibition thus allowing the active confirmation to take place. The ring-shaped FH2 domain initiates actin filament assembly by nucleating actin monomers. The FH1 domain recruits profilin-bound actin monomers to accelerate elongation, contributing to the formation of unbranched actin filaments together with the FH2 domain.

1.8 Rationale and Specific Aims

1.8.1 Rationale for mDia1-RhoA

Our preliminary work has shown that mDia1 knockout (KO) mice exhibit increased plasma osmolality and decreased urine osmolality under basal physiological conditions (Figure 7). Therefore, we hypothesize that mDia1-KO mice have a defect in the osmotic control of VP secretion, resulting in insufficient water retention by the kidney, thus leading to more diluted urine and concentrated blood. Furthermore, mDia1-KO mice exhibit a significantly increased plasma osmolality in response to 2M NaCl injections compared to their wild-type littermates, which is in agreement with our hypothesis that mDia1-KO mice have impaired VP release and impaired homeostatic responses to high salt. In addition, another study reported that mDia1-KO mice show signs of dehydration and anemia, indicated by pale ears and feet [190]. However, it is possible that whole-body mDia1-KO mice also have other defects that can result in impaired homeostatic responses. For example, mDia1-KO mice can exhibit impaired natriuresis and diuresis mediated by mDia1-induced defects in the kidney, which can lead to abnormal plasma and urine osmolality.

As mDia1 is involved in regulating both actin filaments and MTs in a variety of cell types, we hypothesize that mDia1 contributes to the increased osmosensitivity of VP neurons in SL by increasing cytoskeleton density. Previous work in the lab has shown that mDia1 is enriched in the SON compared to other brain areas in the baseline condition (Figure 8). Moreover, mDia1 has been shown to increase beneath the plasma membrane of VP neurons in the SON and PVN following 7 days of SL (Figure 9).

Likewise, Zhang & Bourque showed in 2008 that Ang II enhances the intrinsic osmosensitivity of magnocellular SON neurons by increasing actin filament density via G-

protein-coupled receptors (GPCRs) and PKC/PLC pathway (Figure 10) [99,191]. PKC can increase actin filament density in dendrites of hippocampal neurons by activating Rac1 and RhoA [192]. Additionally, GPCR has been shown to mediate Rho GTPase activation [193–196], and Ang II causes a rapid Rho-mediated increase in actin filament density in HEK293 cells, cardiac myocytes, and mesothelial cells [197–199]. Previous studies have also indicated that Ang II increases the expression levels of GEFs which can lead to activation of RhoA [200–203]. Additionally, studies in non-neuronal cells established that mDia1 is one of two major direct downstream effectors of RhoA. Thus, RhoA might be a signaling molecule that modulates actin filament density upstream of mDia1 in magnocellular VP neurons.

In conclusion, we hypothesize that SL can activate the RhoA-mDia1 pathway to increase the cytoskeletal density and intrinsic osmosensitivity of magnocellular VP neurons, leading to excessive VP secretion, fluid retention, and vasoconstriction, resulting in an increase in blood volume, peripheral resistance, elevated BP, and thereby contributing to hypertension.

1.8.2 Specific Aims

To evaluate if the elevated density of actin filaments and MTs in SL is mediated by increased synthesis of actin and tubulin monomers, our first aim is to assess the expression levels of β-actin and βIII-tubulin in the SON upon SL by western blotting. If we observe increased expression levels of β-actin and βIII-tubulin in the SON following SL, it will suggest that the elevated density of actin filaments and MTs in SL is due to increased expression of actin and tubulin, which leads to the elevation of the concentration of actin and tubulin monomers, thus shifting the dynamics towards polymerization of new actin filaments and MTs. However, if we observe no difference in β-actin and βIII-tubulin expression levels between control and SL rats, this will indicate that the concentration of actin and tubulin monomers remains unchanged, and

the increased density of actin filaments and MTs is a result of SL-induced activation of actin and/or MT polymerizing molecules. Second, using immunohistochemistry and western blot, we will examine if mDia1 and RhoA expression levels in VP neurons are changed following SL. Our first hypothesis is that the expression levels of mDia1 and RhoA will increase in VP neurons in response to SL. An alternative hypothesis is that mDia1 and RhoA levels are not altered in VP neurons following SL, but their activation levels increase, which may lead to the elevated density of actin filaments and MTs in SL. Third, to examine if mDia1 activation mediates cytoskeletal changes in SL, we will inhibit mDia1 activation by intracerebroventricular (icv) injections of small molecule inhibitor of formin homology 2 domains (SMIFH2) during SL. We hypothesize that increases in actin network density in VP neurons in SL will be inhibited by SMIFH2. Moreover, we will evaluate actin cytoskeleton structures in rats chronically exposed to mildly elevated sodium chow. We expect that SL will increase actin density compared to rats fed a control diet. Lastly, we aim to identify additional molecular pathways that might contribute to the unique cytoskeleton networks found in the SON by analyzing the proteome of the rat SON and cortex using mass spectrometry.

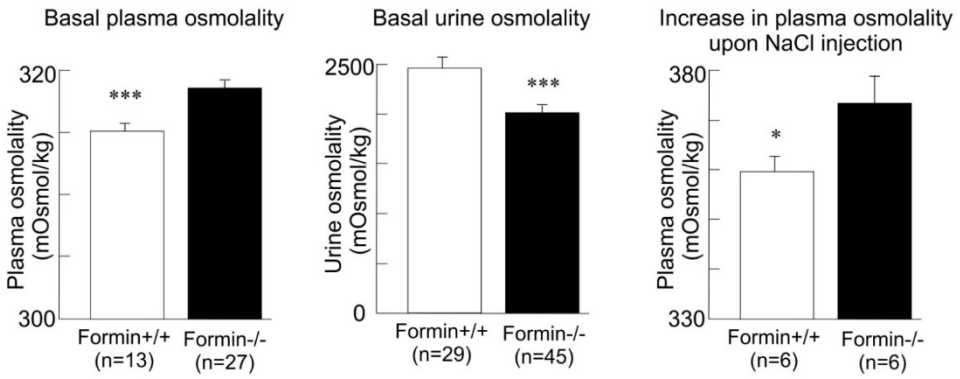

Figure 7. Impaired fluid balance in mDia1-knockout (KO) mice.
A) Basal plasma osmolality and **B)** basal urine osmolality in mDia1-KO mice and their WT littermates. **C)** Plasma osmolality 30 minutes following acute 2M NaCl injection. Data are reported as mean ± SEM. (***p < 0.001, ****p < 0.0001).

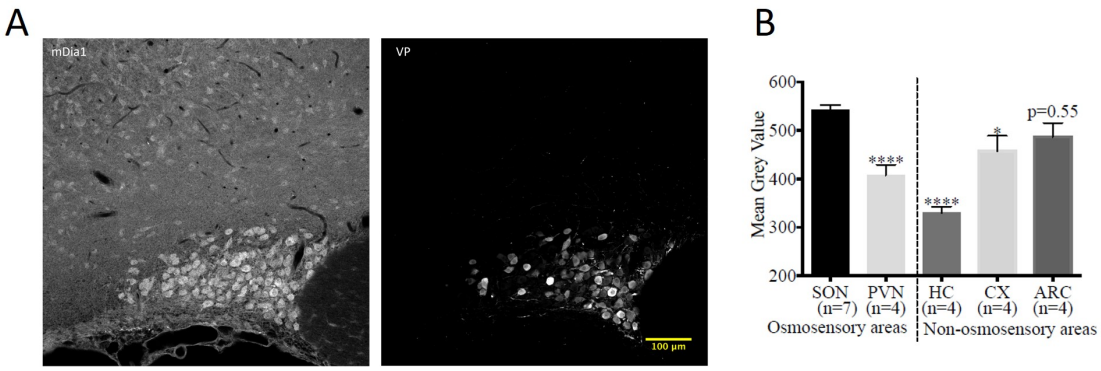

Figure 8. mDia1 is enriched in the SON compared to other brain regions.
A) Immunostaining shows that mDia1 is enriched in the SON harboring VP neurons (left panel shows mDia1, right panel VP). **B)** mDia1 expression levels are significantly higher in the SON compared to other brain regions: PVN, hippocampus (HC), cortex (CX), but not arcuate nucleus (ARC). SON (n = 7); PVN, HC, CX, and ARC (n = 4). Data are reported as mean ± SEM. (*p < 0.05, ****p < 0.0001). (Unpublished data obtained by Suleima Jacob-Tomas, Prager-Khoutorsky lab).

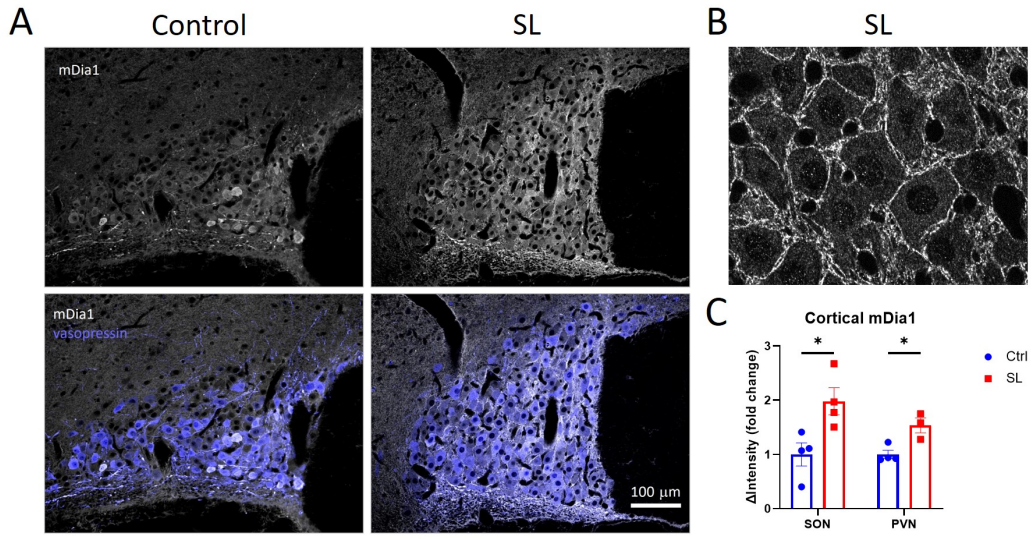

Figure 9. SL increases mDia1 cortical levels in VP neurons.
A) Immunostaining of mDia1 (white) and VP (blue) in the SON from control and SL rats. **B)** mDia1 is enriched beneath VP neuron's plasma membrane in SL. **C)** mDia1 shows significantly higher submembrane levels in the SON and PVN VP neurons from SL rats compared to control rats. SON: control (n = 4 rats); SL (n = 4 rats). PVN: control (n = 4); SL (n = 3). (*p < 0.05). (Unpublished data obtained by Suleima Jacob-Tomas, Prager-Khoutorsky lab).

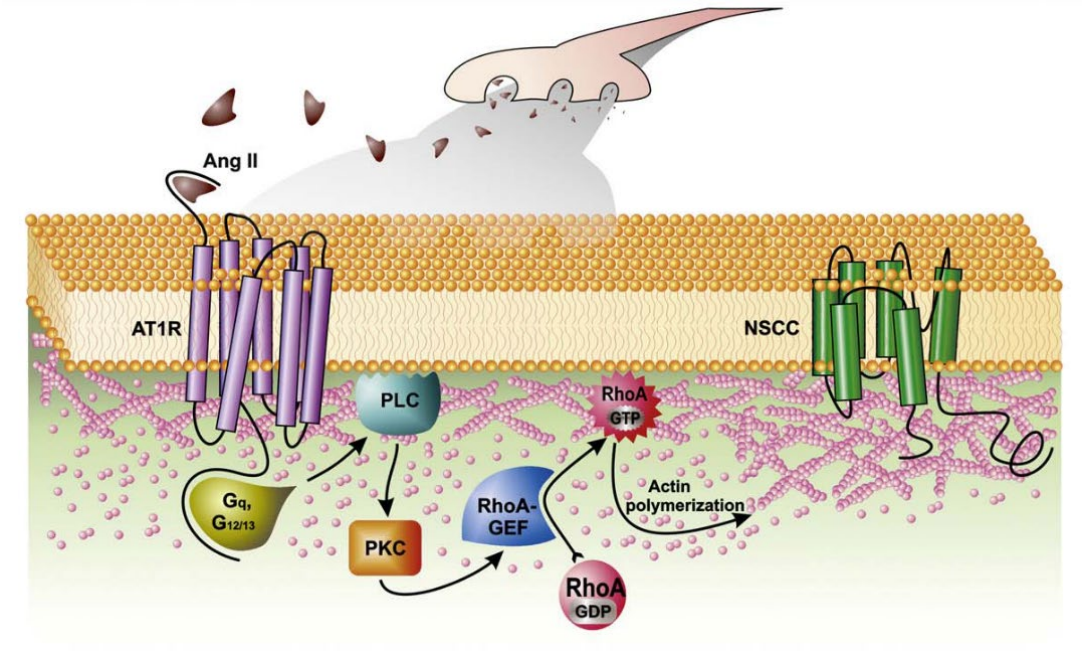

Figure 10. Schematic diagram of the hypothetical pathway describing angiotensin II (Ang II)-mediated enhancement of intrinsic osmosensitivity in SON VP neurons.
Ang II released by afferent nerve terminals binds to AT1 receptor (AT1R) coupled to G proteins such as G_q or/and $G_{12/13}$. G protein activation is mediated by PLC/PKC pathway to enhance the intrinsic osmosensitivity of SON VP neurons mediated by an increase in actin filament density. We hypothesized that RhoA is activated downstream of PLC/PKC by a RhoA-specific guanine nucleotide exchange factor (RhoA–GEF), such as p115RhoGEF or leukemia-associated Rho guanine–nucleotide exchange factor (LARG). Activated RhoA then triggers an increase in actin polymerization to elevate actin filament density, thus contributing to enhanced intrinsic osmosensitivity. (Adopted from Prager-Khoutorsky & Bourque, *Trends in Neurosciences,* 2010).

2. Methods

2.1 Animals

Male and female Wistar rats (250-350 g; Charles River Laboratories, Wilmington, MA, USA) were used throughout the study and treated in strict accordance with the guidelines outlined by the Canadian Council on Animal Care (http://www.ccac.ca), and the experiments adhered to protocols #AUP7948 approved by the Facility Animal Care Committee (FACC) of McGill University. All rats were housed individually and kept under a 12:12 hour light/dark cycle (light 7 AM-7 PM). Food and water were provided *ad libitum*.

The estrus cycle of female rats used in 3.3.2 (RhoA expression in the SON following SL) was tracked using vaginal smearing. Vaginal smears were obtained with a micropipette. The tip of the micropipette was filled with 100 µl saline (0.9%). Then the tip of the micropipette was inserted into the vagina of the female rat and obtained vaginal smears. The vagina was flushed 2-3 times with the saline and then the fluid was placed on a slide with a coverslip. The phase of the estrus cycles was then determined based on the types and the proportion of obtainedcells using a light microscope (20x) [204].

2.2 Salt-loading (SL)

SL is one of the best-characterized HDS-induced rodent models of hypertension. SL involves replacing drinking water with 2% NaCl for 7 days. Rats exposed to 7 days of SL increase their fluid consumption, and display elevated plasma osmolality [103] and BP [73]. Studies have revealed that elevated mean arterial pressure following SL can be attenuated with a V1R antagonist, implying that excessive VP release contributes to the increased BP in this model of salt-sensitive hypertension [73].

In the present study, both control and SL rats were fed standard chow with 0.4% NaCl *ad libitum.* Prior to the start of SL, all animals were habituated to single housing for at least 1 week. During the SL process, fluid consumption was measured daily by weighing the drinking bottles. Blood samples were collected prior to transcardiac perfusion by the end of SL to measure plasma osmolality. The blood collection procedure was performed as previously described [205]. Blood was taken from the left atrium just before the perfusion tube was inserted into the right ventricle. Blood samples were placed on ice for ~ 1 hour before centrifuging at 10000 rpm for 5 minutes at 4°C. Then serum samples were collected for measuring osmolality using a single-sample Micro Osmometer in triplicates.

2.3 Chronic exposure to elevated sodium chow

Animals were fed with 2% or 4% NaCl chow or control standard 0.4% NaCl chow for 2 months, with drinking fresh water provided *ad libitum.* In contrast to the salt-Ang hypertension model [206–209] or the DOCA-Salt hypertension model [210], the animals did not develop increased BP [211–213]. The animals also did not show increased plasma osmolality. Compared to SL, this protocol is more clinically relevant as it better mimics the HDS consumption situation happening in humans.

2.4 Intracerebroventricular (icv) injection of formin inhibitor small molecule inhibitor of formin homology 2 domains (SMIFH2)

Using isoflurane-induced anesthesia, chronic icv cannulas were implanted into the left ventricle according to coordinates 0.15 mm caudal, 1.5 mm lateral to bregma, and 3.5 mm below the skull surface. The cannulas were secured by dental cement, and three stainless steel screws were used to anchor them to the bone. Rats were housed individually for a week after surgery and handled daily to habituate them with the injection procedure to minimize stress.

SMIFH2 (Cat#ab218296, Abcam, USA) was dissolved in DMSO and stored as a stock solution (10 mg/ml) at -80ºC until use. On the day of the experiment, SMIFH2 was diluted in DMSO (50% of the final volume) and Poly(ethylene glycol) 300 to a final concentration of 5 mM and 10 mM on the day of the experiment.

For both vehicle and drug-treated groups, icv injections started two days before SL and continued daily during the course of SL. All injections were given intracerebroventricularly in a volume of 6 µl using a microsyringe connected to the injection cannula via polyethylene tubing. 6 µl of the solution was slowly injected over a period of 10 min to allow diffusion of the drug into the cerebrospinal fluid (CSF). To ensure complete delivery of the solution, the injection cannula was left in place for an additional minute before being removed. Animals treated with 5 mM SMIFH2 were salt loaded for 7 days whereas animals treated with 10 mM SMIFH2 were salt loaded for 5 days.

2.5 Immunohistochemistry on tissue sections

Rats were anesthetized and transcardially perfused with 10 ml PBS and then 250 ml PBS containing 4% paraformaldehyde and 0.5% glutaraldehyde at 37°C, pH adjusted to 6.8. To avoid osmotic changes in the brain triggered by perfusion solutions, control rats were perfused with a solution adjusted to 300 mosmol/kg, whereas SL rats were perfused with a solution adjusted to 330 mosmol/kg. Brains were extracted carefully and postfixed for 28-72 h. Coronal sections (50 µm thick) were obtained using a vibratome.

In order to quench the autofluorescence at the 488 nm channel caused by glutaraldehyde during perfusion, sections were then treated for 15 min with 0.1%$NaBH_4$ in ice-cold cytoskeletal buffer containing: 130 mM NaCl, 10 mM MES, 5 mM EGTA, 5 mM $MgCl_2$, and 5mM $MgCl_2$, pH 6.3.

Following incubation with 10% normal goat serum in PBS containing 0.3% Triton X-100 for 1 h, sections were incubated with primary antibodies diluted in PBS containing 0.3% Triton X-100 at 4°C for 24-48 h. After washing with PBS containing 0.3% Triton X-100 3 times, 10 min each, sections were incubated with fluorescently-labeled secondary antibodies (1:500) and 4',6-diamidino-2-phenylindole (DAPI) (dilution 1:5000, Cat#D1306, Invitrogen, USA) for 1.5 h. Then sections were washed with PBS containing 0.3% Triton X-100 3 times, 10 min each, and mounted on coverslips using ProLong Gold Antifade reagent (Cat#P36930, Invitrogen, USA) and imaged using LSM 880 with AiryScan (Zeiss).

Primary antibodies used in this study are: beta-Actin mouse monoclonal antibody (Cat#A5441, Sigma, 1:500), vasopressin guinea pig polyclonal antibody (Cat#403004, SYSY, 1:1000), RhoA rabbit polyclonal antibody (Cat#2117S, CST, 1:100), mDia1 rabbit polyclonal antibody (Cat#20624-1-AP, Proteintech, 1:50).

Secondary antibodies used are: Alexa Fluor 568 goat anti-rabbit (Cat#A11036, Invitrogen, USA), Alexa Fluor 488 goat anti-mouse (Cat#A11029, Invitrogen, USA), Alexa Fluor 647 goat anti-guinea pig (Cat#A21450, Invitrogen, USA).

2.6 Confocal microscopy with AiryScan

Confocal images were acquired by LSM 880 (Zeiss) using Plan-Apochromat 20x/0.8 M27 objective and Plan-Apochromat 63x/1.40 Oil DIC M27 objective. Sections were examined in 4 channels (405 nm, 488nm, 568nm, and 647 nm). For 20x magnification, stacks of 20-35 optical planes (1 μm step) were acquired. For 63x magnification, stacks of 28-36 optical planes (0.3 μm step) were acquired.

Airyscan imaging was conducted using Plan-Apochromat 63x/1.40 Oil DIC M27 objective and the AiryScan super-resolution (SR) module with a 32- channel hexagonal array

GaAsP-PMT area detector. Stacks containing 15-25 optical sections (179 nm step) were acquired consecutively in 4 channels as above. Airyscan super-resolution images were reconstructed using SEN Black software (Zeiss). Confocal and Airyscan images were analyzed using SEN Blue software (Zeiss) and FIJI ImageJ (NIH).

2.7 Western blotting

Extracted tissue was homogenized and lysed in RIPA lysis buffer (Cat#89900, Thermo Scientific, USA) on ice with EDTA-free protease inhibitor (Cat#4693132001, Sigma-Aldrich, USA), phosphatase inhibitor cocktail 2 (Cat#P5726-1ML, Sigma-Aldrich, USA, 1:100), and cocktail 3 (Cat#P0044-1ML, Sigma-Aldrich, USA, 1:100). Following centrifugation at 10,000 g for 10 min, the supernatant protein concentration was measured by Pierce BCA Protein Assay Kit (Cat#23227, Thermo Scientific, USA). 15-40 mg of protein was loaded on 10% TGX Stain-Free FastCast gel (Cat#1610183, BIO-RAD, USA). Following electrophoresis, proteins were transferred to 0.2 mm nitrocellulose membranes. Membranes were blocked in 5% BSA in Tris-buffered saline containing 0.1% Tween-20 (TBS-T) for 1 h at room temperature prior to overnight incubation with primary antibodies. Following three washes with TBS-T, the membranes were incubated for 1 h with HRP-conjugated secondary antibodies (1:5000 in 5% BSA), washed again, treated with Enhanced Chemiluminescent (ECL) reagent, and visualized using a ChemiDoc Imaging System (Bio-Rad).

Western blot results were normalized based on total lane protein using the stain-free gel technology (Cat#1610183, BIO-RAD, USA). The gel formulation incorporates a trihalo compound that can covalently bind to tryptophan residues and enhance protein fluorescence when exposed to UV irradiation [214]. This enables the detection of proteins at levels as low as 10-25 ng [214]. Lane and band analysis was done in Image Lab. Normalization factor = total

volume (intensity) stain-free reference lane / total lane stain-free volume (intensity) of each lane. Normalized volume (intensity) was obtained by normalization factor x volume (intensity).

Primary antibodies used for western blotting are: mDia1 rabbit polycloncal antibody (Cat#ab189840, abcam, 1:2000), betaIII-tubulin monoclonal antibody (Cat#8578, Sigma, 1:100), beta-Actin mouse monoclonal antibody (Cat#A5441, Sigma, 1:5000), RhoA rabbit polyclonal antibody (Cat#2117S, CST, 1:1000).

2.8 Mass spectrometry

Tissue extraction and sample preparation were done as described for western blotting. 10-20 μg of proteins per sample were prepared for mass spectrometry processing. All mass spectrometry experiments were conducted on an Orbitrap Fusion™ Tribrid™ Mass Spectrometer (Thermo Fisher Scientific) in collaboration with the Proteomics Platform of the McGill University Health Centre (RI-MUHC). Proteins were identified based on the Uniprot Rat canonical sequence database. Raw data were viewed and analyzed by Scaffold software.

2.9 Statistical analysis

2.9.1 Fluid intake during SL

Daily fluid intake was measured and assessed by two-way ANOVA followed by Sidak's multiple comparisons test in Graphpad Prism 8. Cumulative drinking over 7 days and serum osmolality were assessed by a two-tailed, unpaired, parametric Student's t-test. The significance level was set at $p<0.05$. *$p<0.05$, **$p<0.01$, ***$p<0.001$, and ****$p<0.0001$.

2.9.2 mDia1 and RhoA cytoplasmic levels analysis

Maximal projections of z-stacks (10 consecutive images for mDia1, 6 consecutive images for RhoA) were generated. 20 neurons per rat brain labeled with VP were sampled from the left and right sides of the SON and PVN. Mean grey values for mDia1 and RhoA were measured

within a 4 × 4 μm square using FIJI ImageJ. Statistical analyses were conducted using Graphpad Prism 8. Results are reported as mean ± SEM and assessed using a two-tailed, unpaired, parametric Student's t-test.

2.9.3 mDia1 and RhoA cortical levels analysis

A single optical plane was used to analyze cortical levels. 20 VP neurons per rat were sampled from the left and right sides of the SON and PVN. Line scan profiles were generated using FIJI by placing a perpendicular 8-μm-long line across the cell perimeter. Delta (Δ) Mean grey values were obtained by subtracting the baseline mean grey value at both ends of the line profile from the peak mean grey value. Results are reported as mean ± SEM and assessed using a two-tailed, unpaired, parametric Student's t-test in Graphpad Prism 8.

2.9.4 Actin cytoskeleton analysis

Single Airyscan optical sections were used for analyzing the subcortical actin layer and comets-like actin structures. 10 VP neurons per rat were sampled from the left and right sides of the SON and imaged with Airyscan. Subcortical actin layer intensity was evaluated using line scan profiles which were generated by placing a perpendicular 4-μm-long line across the cell perimeter. The subcortical actin layer intensity was obtained by subtracting the baseline intensity at both ends of the line profile. The subcortical actin layer thickness was calculated based on the line profiles, and the distance around the intensity peak was taken as thickness when fluorescence intensity drops to 50%. The intensity and thickness of the subcortical actin layer in each cell were calculated by averaging three-line profiles per cell.

The density of comet-like actin structures in the cytoplasm was obtained by counting the number of comet-like actin filaments in a 4 × 4 μm square. The length of comet-like actin structures was calculated by averaging 8 actin filaments in the 4 × 4 μm square. Note that the

length of comets-like actin structures might be underestimated since they can extend through multiple optical sections on the z-axis.

3. Results

3.1 Increased fluid intake and elevated plasma osmolality during 7 days of SL

The daily fluid intake and overall fluid intake of salt-loaded rats (n = 20, 4 females, 16 males) and control rats (n = 20, 4 females, 16 males) were measured during 7 days of salt loading. Daily fluid intake was assessed by two-way ANOVA. Post-hoc multiple comparison test showed significantly increased fluid consumption in SL rats starting from day 2 (day 1 $p = 0.8014$; day 2 $p = 0.0065$; day 3 $p = 0.0002$; day 4-7 $p < 0.0001$, Figure 11A). Overall fluid intake during 7 days was assessed by Student's t-test. The data showed a significantly increased cumulative drinking in 7 days in SL rats ($p < 0.0001$, Figure 11B). Following the SL, blood samples (~1 mL per animal) were collected. Blood serum was prepared following centrifugation for measuring plasma osmolality. Plasma osmolality was significantly increased in SL rats compared to control rats (321.3 mOsmol/kg ± 3.751 and 301.6 mOsmol/kg ± 0.8838 respectively, $p < 0.0001$, Figure 12). These results are consistent with previous studies characterizing these parameters in SL rats [59, 159,160].

3.2 Expression levels of β3-tubulin and β-actin in the supraoptic nuclei (SON) do not changes following SL

Two hypotheses can explain the increased density of actin filaments and MTs in SON VP neurons after SL. The first hypothesis suggests that the increased density of actin filaments and MTs in SL is due to increased expression of actin and tubulin, elevating the concentration of actin and tubulin monomers, which shifts the dynamics towards polymerization of new actin filaments and MTs. The second hypothesis implies that the concentration of actin and tubulin

monomers remains unchanged, and the density of actin filaments and MTs increases due to SL-induced activation of actin and/or MT polymerizing molecules. To investigate which hypothesis better explains our observations in SON VP neurons upon SL, western blot was done to compare the overall expression levels of β-actin and β3-tubulin in the SON between control and SL rats.

β-actin and β3-tubulin expression levels were examined in SONs from SL (n = 5, male, for β-actin; n = 4, male, for β3-tubulin) and control (n = 4, male, for both β-actin and β3-tubulin) rats. Since in these experiments β-actin and β3-tubulin were proteins of interest, they could not serve as housekeeping genes. Therefore, instead of using housekeeping genes as loading controls, we adopted another unbiased and well-characterized strategy to normalize western blot results based on the total lane protein. No significant difference was observed in both β-actin and β3-tubulin expression between control and SL (Figure 13). The results support the second hypothesis, suggesting that the increased density of actin filaments and MTs in VP neurons of SL rats can be due to the shifted balance to promote polymerization induced by the SL-induced activation of actin and/or MT polymerizing molecules, and not due to the overall increases in actin and tubulin levels.

3.3 mDia1 and RhoA cortical levels increase in VP neurons following SL

3.3.1 mDia1 expression in the SON and paraventricular nuclei (PVN) following SL

Based on experiments conducted by Suleima Jacob-Tomas's Master's thesis, mDia1 expression levels might be elevated close to the surface of VP neurons in the SON and PVN following SL. To confirm this observation, we evaluated mDia1 cytoplasmic and cortical levels in magnocellular VP neurons using another mDia1 antibody (Cat#20624-1-AP, Proteintech, USA) in a larger sample size, and including both male and female rats. mDia1 expression levels were compared in SL and control rats in the SON (n = 10, 4 females, 6 males; n = 10, 4 females,

6 males respectively) and PVN (n = 6, 3 females, 3 males; n = 6, 3 females, 3 males respectively). mDia1 cortical expression levels were about 1.8 fold higher in SON VP neurons in SL rats as compared to control rats ($p = 0.0001$, Figure 14A-C). Likewise, mDia1 cytoplasmic levels were about 1.5 fold higher in SON VP neurons in SL rats as compared to control rats ($p = 0.0001$, Figure 14A, B, D). Similarly, mDia1 cortical expression levels were about 1.6 fold higher in PVN VP neurons in SL rats as compared to control rats ($p = 0.0004$, Figure 15A-B). However, mDia1 cytoplasmic levels did not show a significant change in PVN VP neurons in SL rats ($p = 0.1623$, Figure 15A, C). No significant difference was detected between male and female rats, thus data from both sexes were pulled together (Figure 14-15). mDia1 has been proved to localize to the plasma membrane upon activation in non-neuronal cells in culture [162–164]. Therefore, we hypothesize that mDia1 activation levels increase in VP neurons following SL.

3.3.2 RhoA expression in the SON following SL

mDia1 has been identified as one of the downstream effectors of RhoA [139]. Both mDia1 and RhoA have been shown to translocate to the plasma membrane upon activation in non-neuronal cells [162–165]. Therefore, we assessed RhoA expression levels in VP neurons in SL rats. RhoA expression levels were evaluated in SL and control rats in the SON (n = 15, 5 females, 10 males; n = 13, 5 females, 8 males respectively). RhoA cortical expression levels were about 1.7 fold higher in SON VP neurons in SL rats as compared to control rats ($p < 0.0001$, Figure 16A-C), while RhoA cytoplasmic expression levels did not significantly change in SON VP neurons in SL rats ($p = 0.0616$, Figure 16A, B, D). We initially observed a high variability in RhoA expression in the SON in female rats. Previous research has shown that estrogen can activate RhoA and phosphorylates (and thereby inactivates) the actin severing

protein cofilin in the hippocampus [215]. Therefore, it is possible that fluctuations in the estrogen levels during the estrous cycle cause variability in the RhoA expression levels in the SON in female rats. To reduce the variability, the estrous cycle of female rats was tracked, rats were synchronized, and brains were collected during the diestrous phase which has the lowest estrogen levels.

The above findings indicate that the activation of RhoA-mDia1 signaling is potentially increased in VP neurons following SL. RhoA activation in VP neurons upon SL will be further validated by pull-down assays for activated RhoA GTPases.

3.4 No change in total RhoA and mDia1 expression levels in the SON following SL

To determine if the elevated RhoA and mDia1 expression levels caused by SL observed in immunohistochemistry results were caused by upregulated activation, but not by an overall increased expression of RhoA and mDia1, we performed western blot analysis on lysates of SON tissue obtained from control and SL rats. Total RhoA and mDia1 expression levels were evaluated in SL and control rats in the SON (n = 4, male; n = 4, male respectively). No difference was observed in both total RhoA and mDia1 (Figure 17). The results suggest that SL increases the activation of RhoA and mDia1 in magnocellular VP neurons, which may lead to the upregulation of the polymerization of the actin and MT networks.

3.5 Actin cytoskeleton density decreases in SON VP neurons from SMIFH2-treated rats in SL

To investigate the effect of preventing mDia1 activation without changing its overall expression levels, formin inhibitor SMIFH2 was injected icv in rats undergoing SL. SMIFH2 binds to the catalytic domain (FH2) of formins, inhibiting its effects on actin and MT polymerization (Figure 18A) [216]. The injections were done daily via cannulas implanted into

the lateral ventricle, started two days before initiation of SL, and proceeded during the 7 days of SL. Subcortical actin layer and comet-like actin filaments were analyzed in SON VP neurons *in situ* from vehicle (n = 3, male) and SMIFH2-treated rats (n = 4, male). Results show that SMIFH2 reduced actin structure density under SL compared to the vehicle-treated group (Figure 18B). The density of comet-like actin filaments in SON VP neurons decreased significantly in SMIFH2-treated group compared to vehicle-treated controls (vehicle: 18.61 ± 0.3379 vs SMIFH2: 13.92 ± 0.5672 filaments/4 μm^2, p = 0.0013, Figure 18C). Moreover, the length of comet-like structures also decreased in SMIFH2-treated group (vehicle: 1.198 ± 0.05743 vs SMIFH2: 0.9418 ± 0.02830 μm, p = 0.0072, Figure 18D). Line scan analysis of actin immunofluorescence intensity showed no significant difference in subcortical actin layer intensity in SON VP neurons between vehicle and SMIFH2-treated rats (vehicle: 2510 ± 174.5 vs SMIFH2: 2056 ± 128.6 gray levels (g.l.), p = 0.0840, Figure 18E). However, subcortical actin layer intensity showed a trend to decrease in SMIFH2-treated rats compared to the vehicle-treated group (Figure 18E). In addition, no significant difference was observed in the subcortical actin layer thickness in SON VP neurons upon SMIFH2 treatment (vehicle: 0.2741 ± 0.005847 vs SMIFH2: 0.2598 ± 0.006689 μm, p = 0.1856, Figure 18F). These data suggest that formin activation may contribute to the increased polymerization of the actin cytoskeleton in SON VP neurons upon SL. These results support the hypothesis that SL increases the activation of RhoA and mDia1 in magnocellular VP neurons, which might facilitate the polymerization of the actin and MT networks.

3.6 Actin cytoskeleton density increases in SON VP neurons following chronic exposure to elevated sodium chow

The increased density of actin filaments and MTs are observed in HDS-induced SL hypertension model [103,217]. Rats exposed to SL display increased plasma osmolality [103] and elevated BP [73]. Thus, it is not clear if actin filament and MT density increase is a direct effect of HDS, or it is caused by pathologically increased plasma osmolality and BP. Therefore, we assessed the organization of actin cytoskeleton in rats chronically exposed to mildly elevated sodium chow, which does not lead to an increase in either plasma osmolality or BP [211–213]. Animals were fed 2% or 4% NaCl chow or control chow containing 0.4% NaCl chow for 2 months. Animals had access to drinking water *ad libitum.* This protocol better mimics the HDS consumption situation in humans than SL. Subcortical actin layer and comet-like actin filaments were analyzed in SON VP neurons *in situ* in rats fed control 0.4% chow (n = 4, male), 2% chow (n = 4, male), and 4% NaCl chow (n = 4, male). Our data suggest that actin density in SON VP neurons is increased after chronic exposure to elevated sodium chow (Figure 19A). The density of comet-like actin filaments in SON VP neurons increased significantly in rats exposed to 2% and 4% NaCl chow compared to controls (control: 10.97 ± 0.3333 vs 2% NaCl chow: 13.52 ± 0.1095 filaments/4 μm^2, p = 0.0206; control vs 4% NaCl chow: 15.28 ± 0.7420 filaments/4 μm^2, p = 0.0010, Figure 19B). However, no difference was observed between rats exposed to 2% NaCl chow and 4% NaCl chow (p = 0.0751, Figure 19B). Likewise, comet-like structures appeared to be longer in rats exposed to 2% and 4% NaCl chow (control: 0.8101 ± 0.02566 vs 2% NaCl chow: 0.9987 ± 0.03682 μm, p = 0.0037; control vs 4% NaCl chow: 1.121 ± 0.01103 μm, p = 0.0001, Figure 19C). And comet-like structures in rats exposed to 4% NaCl chow were significantly longer than in rats exposed to 2% NaCl chow (p = 0.0252, Figure 19C). In addition,

subcortical actin layer intensity in SON VP neurons increased in rats exposed to 2% and 4% NaCl chow (control: 549.3 ± 17.41 vs 2% NaCl chow: 836.5 ± 70.66 g.l., p = 0199; control vs 4% NaCl chow: 859.9 ± 55.37 g.l., p = 0.0140, Figure 19D), whereas there was no difference between 2% NaCl chow group and 4% NaCl chow group (p = 0.9480, Figure 19D). No significant difference was observed in subcortical actin layer thickness in SON VP neurons following chronic elevated sodium chow (control: 0.2964 ± 0.01625 vs 2% NaCl chow: 0.3048 ± 0.01443 μm, p = 0.9011; control vs 4% NaCl chow: 0.3371 ± 0.008455 μm, p = 0.1426; 2% NaCl chow vs 4% NaCl chow, p = 0.2178, Figure 19E). Despite that actin cytoskeleton density increases are smaller than reported for in SL rats (Figure 19A) [103], the results above indicate that similar actin cytoskeleton reorganization happens also in rats chronically exposed to mildly elevated sodium chow. This suggests that increased actin polymerization in SON VP neurons is a consequence of HDS intake, and is not triggered by the increased plasma osmolality and elevated BP.

3.7 Analysis of SON and cortex proteome using mass spectrometry

To explore other potential molecular pathways that might be involved in the regulation of unique cytoskeletal structures in the SON, we employed an unbiased approach to analyze the proteome of the rat SON and cortex. SON and cortex lysates from rats (n = 3 males) were prepared after tissue extraction. 10-20 μg of protein per sample were prepared for mass spectrometry processing using an Orbitrap Fusion™ Tribrid™ Mass Spectrometer. Proteins were then identified based on the Uniprot Rat canonical sequence database.

A total of 2647 proteins were identified in the rat SON and cortex, among these proteins, 333 were only detected in the cortex, 362 were only detected in the SON, and 1952 were detected in both (Figure 20A).

Following Student's t-test (considered significant as $p < 0.05$), 496 proteins were significantly increased in the cortex, and 333 proteins were significantly increased in the SON, whereas 1818 proteins showed the same expression levels in both areas (Figure 20 B-C). Further work needs to be done to identify cytoskeleton-related proteins that may contribute to the unique cytoskeletal organization in the SON.

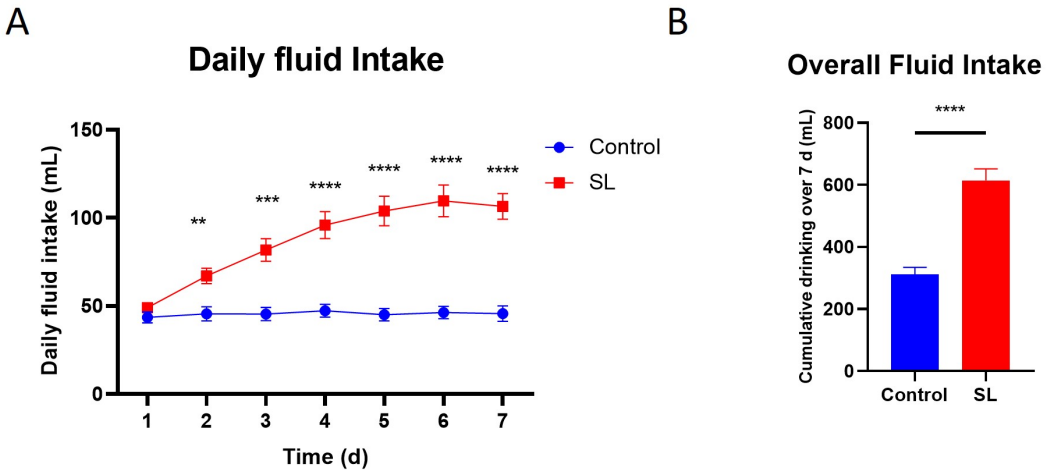

Figure 11. Increased fluid intake during the course of SL.
A) Daily fluid intake was monitored in rats undergoing SL by replacing their drinking solution with 2% NaCl water and in control rats drinking tap water *ad libitum.* **B)** Overall fluid intake during 7 days in SL and control rats. SL (n = 20, 4 females, 16 males); Control (n = 20, 4 females, 16 males). Data are reported as mean ± SEM. (**p < 0.01, ***p < 0.001, ****p < 0.0001).

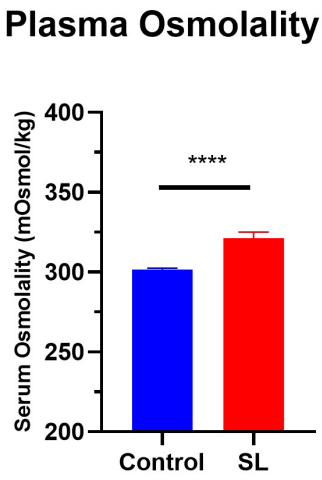

Figure 12. Increased serum plasma osmolality following 7 days of SL.
Serum osmolality after 7-day SL and control rats. SL (n = 20, 4 females, 16 males); Control (n = 20, 4 females, 16 males). Data are reported as mean ± SEM. (****p < 0.0001).

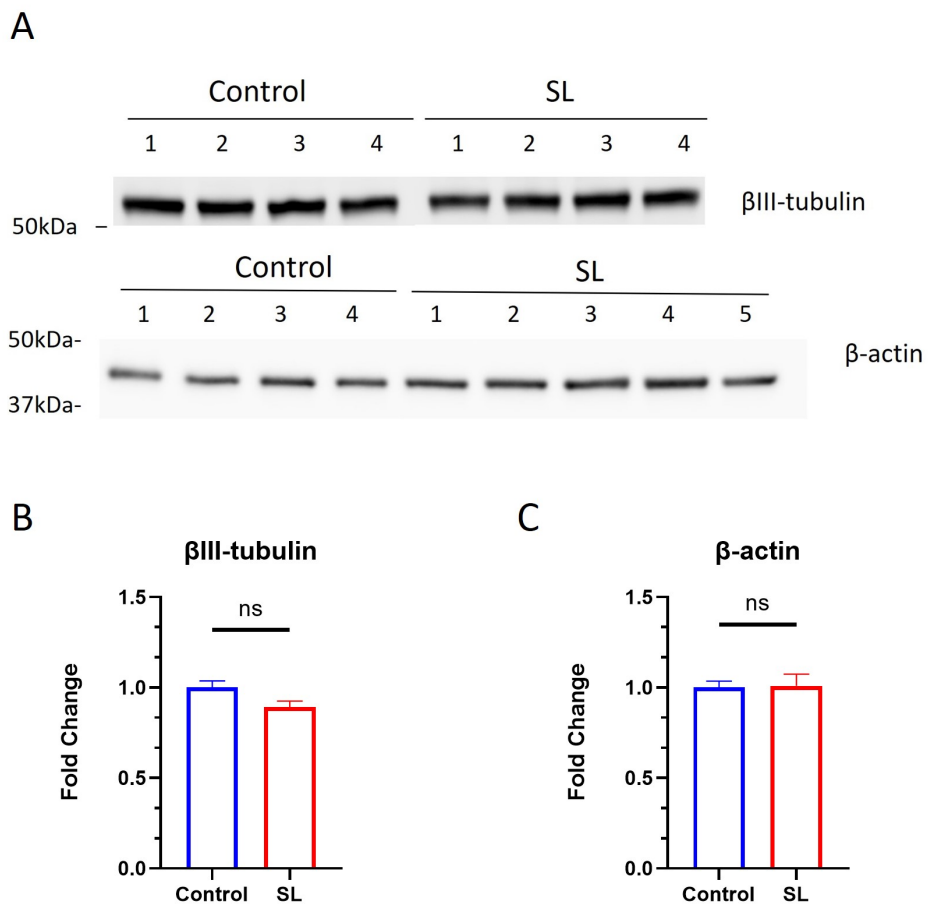

Figure 13. No difference in βIII-tubulin and β-actin expression levels in the SON between control and SL rats.

A) Western blot results show overall βIII-tubulin and β-actin expression levels in the SON between control and SL rats. Results were normalized based on total lane protein. Quantification analysis of βIII-tubulin **(B)** and β-actin **(C)** is shown by bar charts. βIII-tubulin: control (n = 4); SL (n = 4). β-actin: control (n = 4); SL (n = 5). Data are reported as mean ± SEM. (ns: not significant).

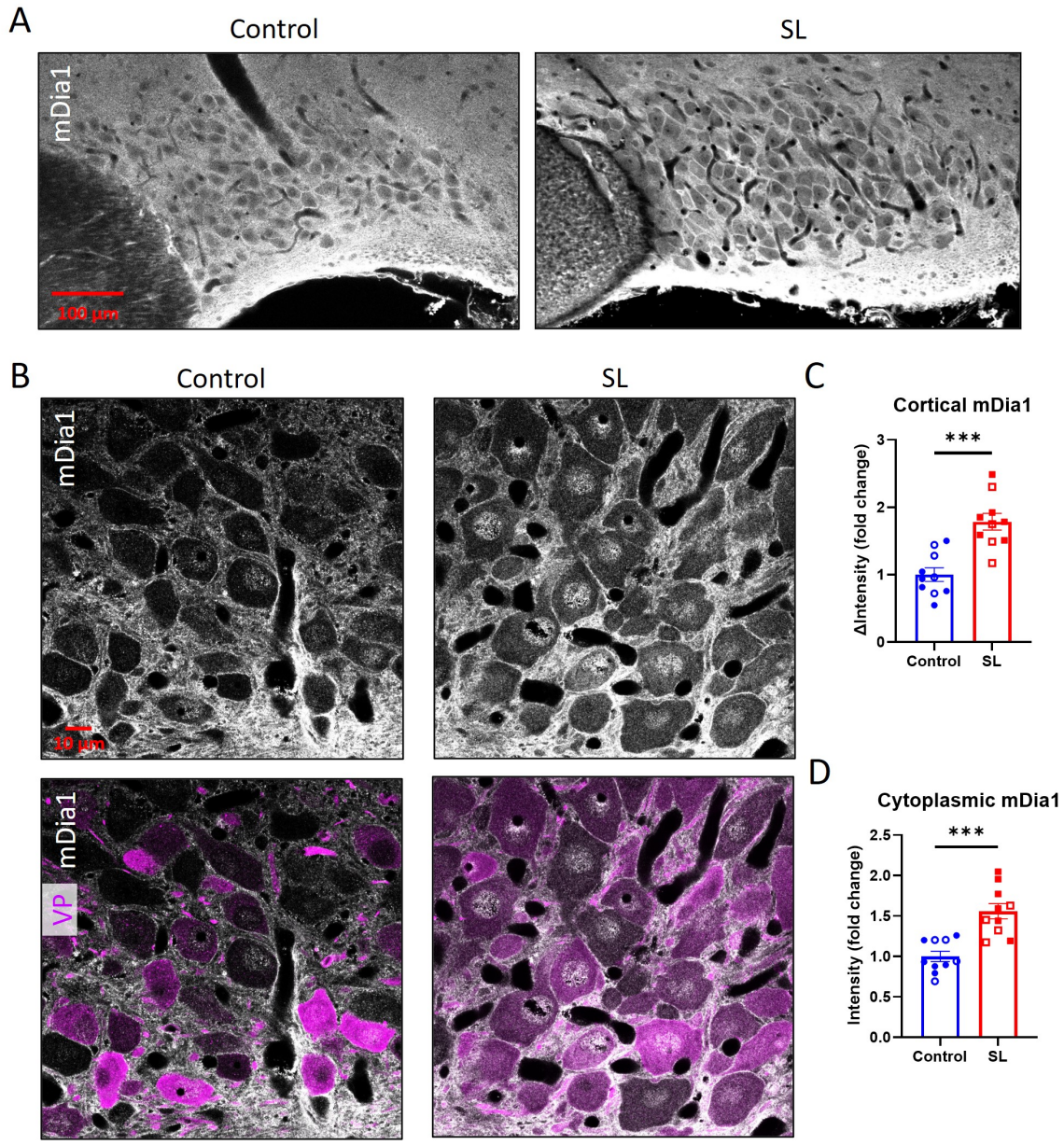

Figure 14. mDia1 cortical and cytoplasmic levels are elevated in SON VP neurons.
A) Immunostaining shows mDia1 (white) organization in the SON from control and SL rats. **B)** High magnification of mDia1 (white) and VP (magenta) in the SON from control and SL rats. **C)** Analysis of cortical mDia1 Δintensity in SON VP neurons between control and SL rats. **D)** Analysis of cytoplasmic mDia1 intensity in SON VP neurons between control and SL rats. 200 VP neurons from 10 control (4 females, 6 males) and 200 from 10 SL (4 females, 6 males) rats were analyzed. Open circles represent data from females, and full circles from males. Data are reported as mean ± SEM. (***$p < 0.001$).

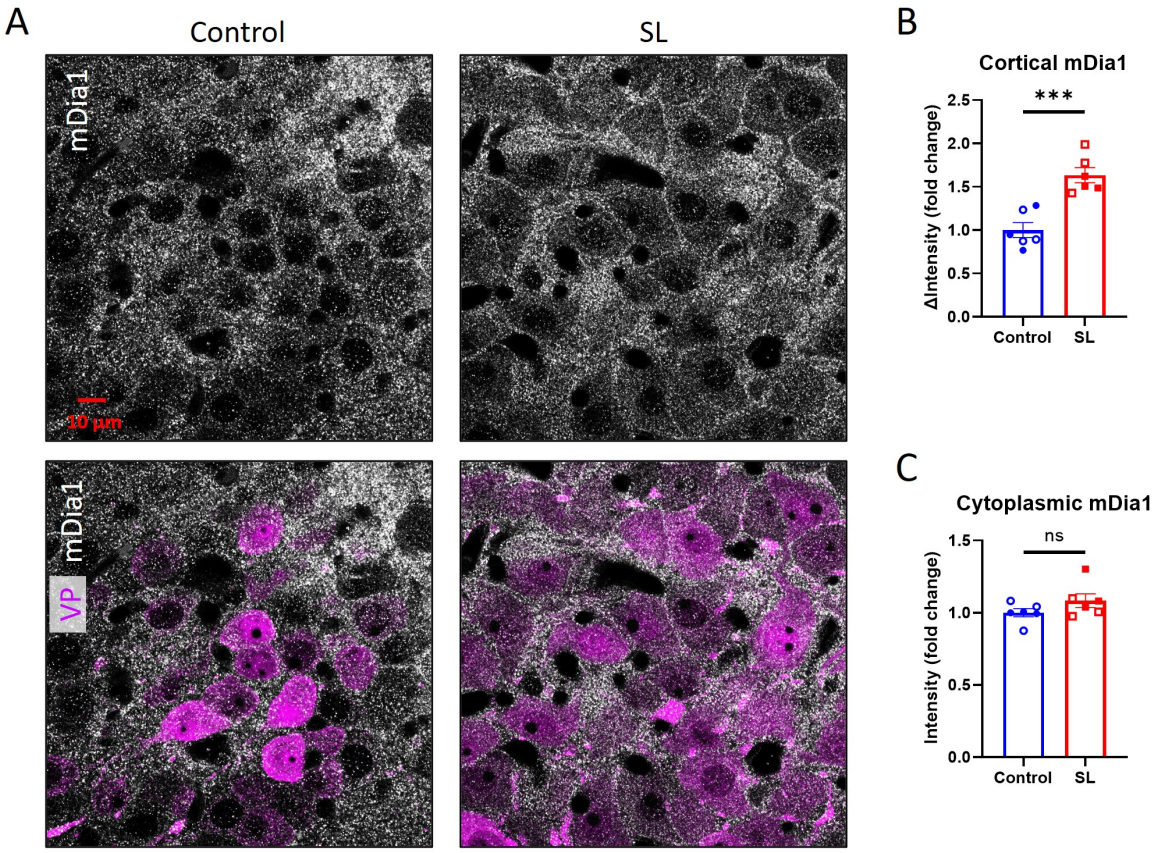

Figure 15. mDia1 cortical levels are elevated in SON VP neurons.
A) High magnification of mDia1 (white) and VP (magenta) in the PVNs from control and SL rats. **B)** Analysis of cortical mDia1 Δintensity in PVN VP neurons between control and SL rats. **C)** Analysis of cytoplasmic mDia1 intensity in PVN VP neurons between control and SL rats. 120 VP neurons from 6 control (3 females, 3 males) and 120 from 6 SL (3 females, 3 males) rats were analyzed. Open circles represent data from females, and full circles from males. Data are reported as mean ± SEM. (ns: not significant, ***$p < 0.001$).

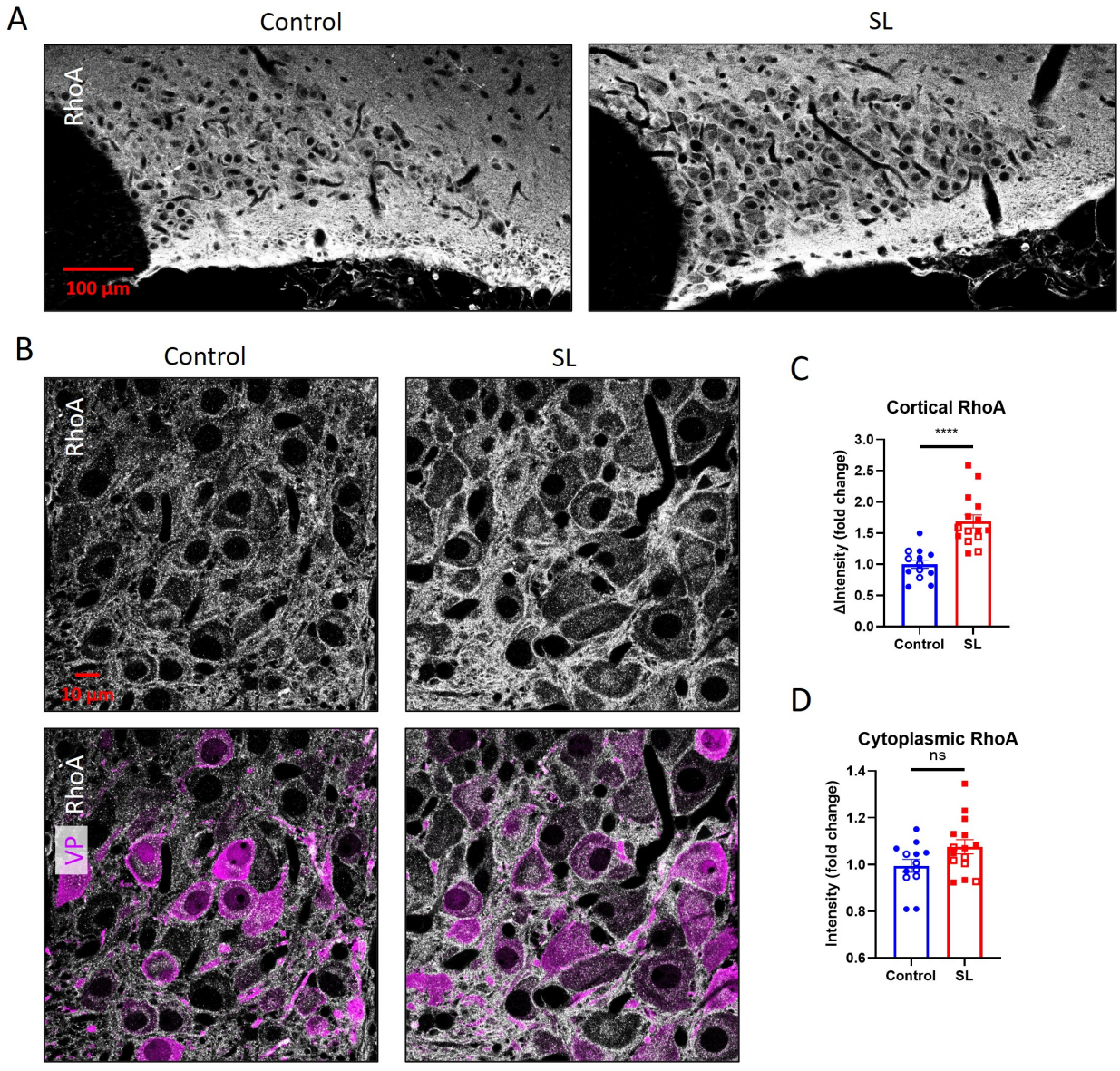

Figure 16. RhoA cortical levels are elevated in SON VP neurons.
A) Immunostaining shows RhoA (white) organization in the SON from control and SL rats. **B)** High magnification of RhoA (white) and VP (magenta) in the SON from control and SL rats. **C)** Analysis of cortical RhoA Δintensity in SON VP neurons between control and SL rats. **D)** Analysis of cytoplasmic RhoA intensity in SON VP neurons between control and SL rats. 260 VP neurons from 13 control (5 females, 8 males) and 300 from 15 SL (5 females, 10 males) rats were analyzed. Open circles represent data from females, and full circles from males. Data are reported as mean ± SEM. (ns: not significant, ***p < 0.001).

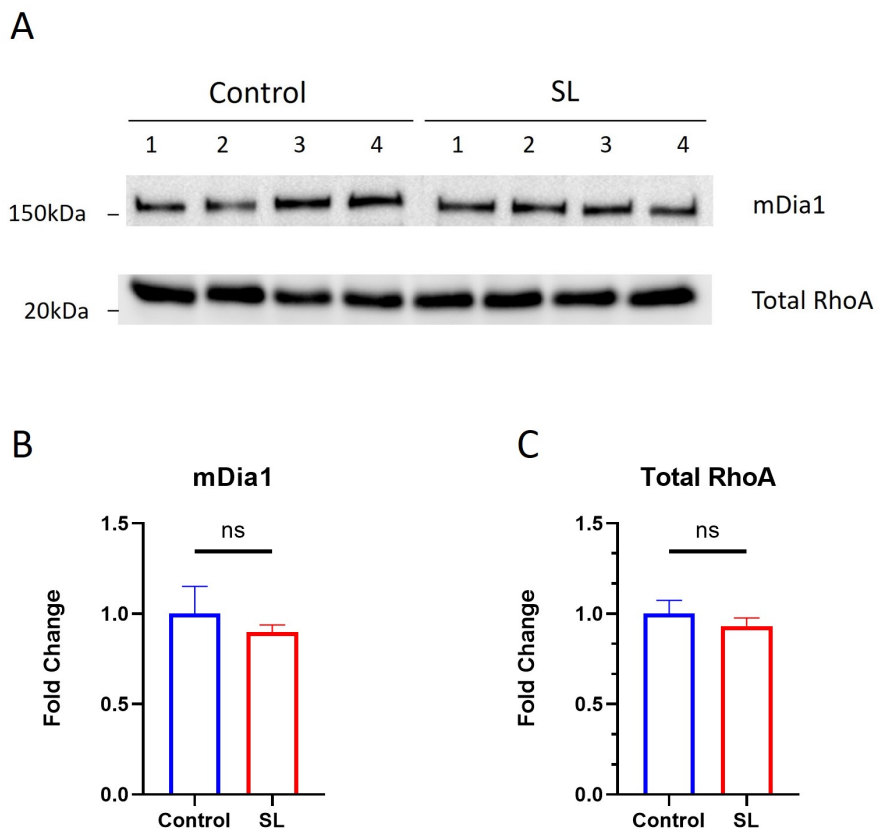

Figure 17. mDia1 and RhoA expression levels in the SON are not different in control vs SL rats. **A)** Western blot results show mDia1 and total RhoA expression levels in the SON between control and SL rats. Results were normalized based on total lane protein. Quantification analysis of mDia1 **(B)** and total RhoA **(C)** is shown by bar charts. SL (n = 4); Control (n = 4). Data are reported as mean ± SEM. (ns: not significant).

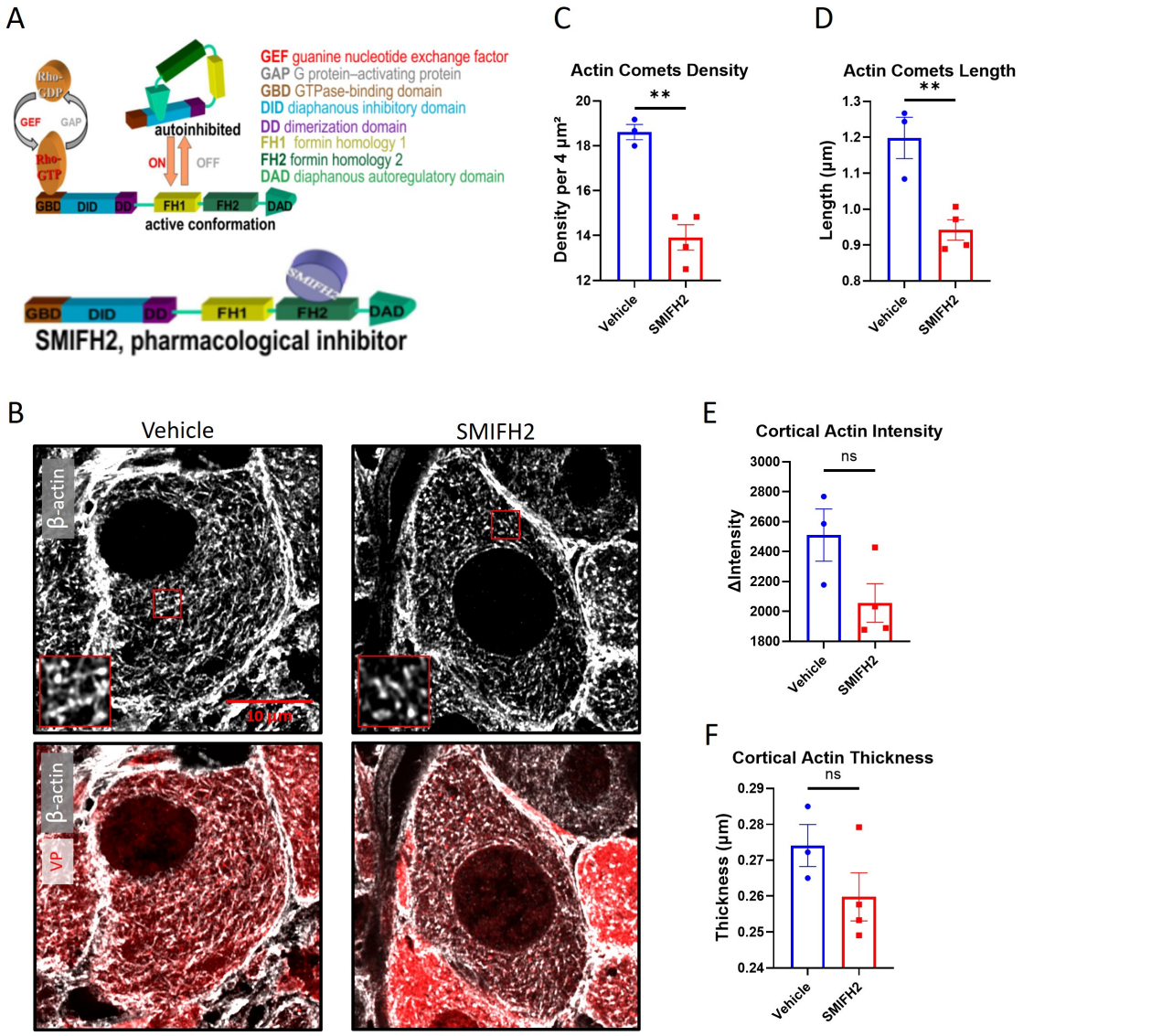

Figure 18. SMIFH2 decreases the density of actin cytoskeleton in SON VP neurons from SL rats.

Vehicle and formin inhibitor SMIFH2 were icv injected into rats undergoing SL. **A)** Schematic illustration of a pharmacological membrane-permeable formin inhibitor SMIFH2. SMIFH2 binds to the FH2 domain to inhibit the catalytic activity of formins and their effects on actin and MT polymerization. **B)** β-Actin (white) and VP (red) in SON VP neurons from control and SL rats were acquired using confocal microscopy with AiryScan. Insets show magnified areas (3 × 3 µm) outlined by red squares on the corresponding images. Mean density **(C)** and mean length **(D)** of comet-like actin structures were quantified in a 4 × 4 µm square within the cytoplasm of SON VP neurons. Mean cortical actin layer intensity **(E)** and mean cortical actin layer thickness **(F)** were evaluated. 30 VP neurons from 3 control (3 males) and 40 from 4 SL (4 males) rats were analyzed. Data are reported as mean ± SEM. (ns: not significant, **p < 0.01).

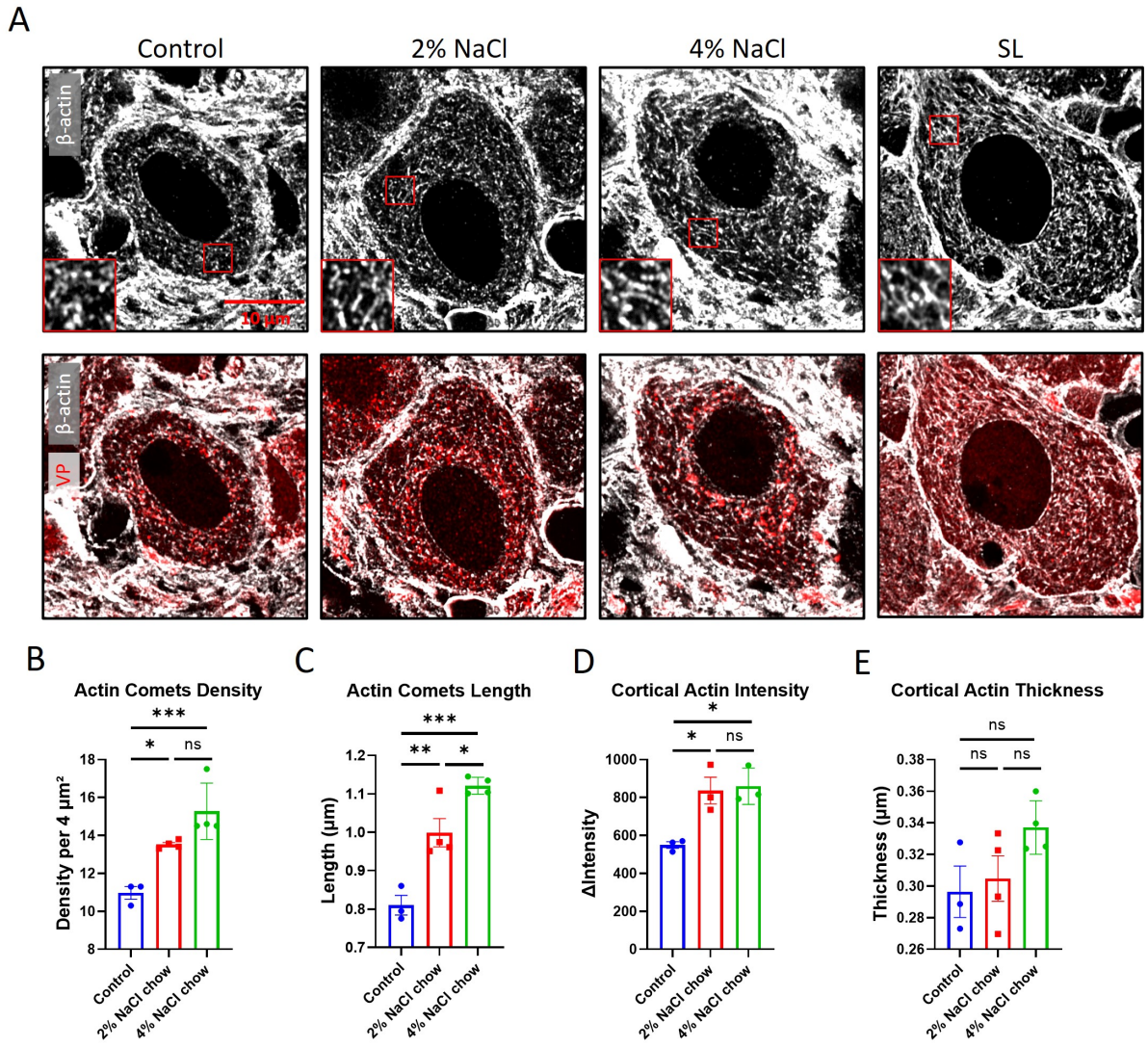

Figure 19. Actin cytoskeleton density is increased in rats chronically exposed to mildly elevated sodium chow.

Rats were fed 2% or 4% NaCl chow or a control standard 0.4% NaCl chow for 2 months, and drinking water was provided *ad libitum*. **A)** β-Actin (white) and VP (red) in SON VP neurons from rats exposed to 2% and 4% NaCl chow compared to control and SL were acquired using confocal microscopy with AiryScan. Insets show magnified areas (3 × 3 µm) outlined by red squares on the corresponding images. Mean density **(B)** and mean length **(C)** of comet-like actin structures were quantified in a 4 × 4 µm square on the cytoplasm of SON VP neurons. Mean cortical actin layer intensity **(D)** and mean cortical actin layer thickness **(E)** were evaluated. 30 VP neurons from 3 control (3 males), 40 from 4 2% NaCl chow exposed (4 males), and 40 from 4 4% NaCl chow exposed (4 males) rats were analyzed. Data are reported as mean ± SEM. (ns: not significant, *p < 0.05, **p < 0.01, ***p < 0.001).

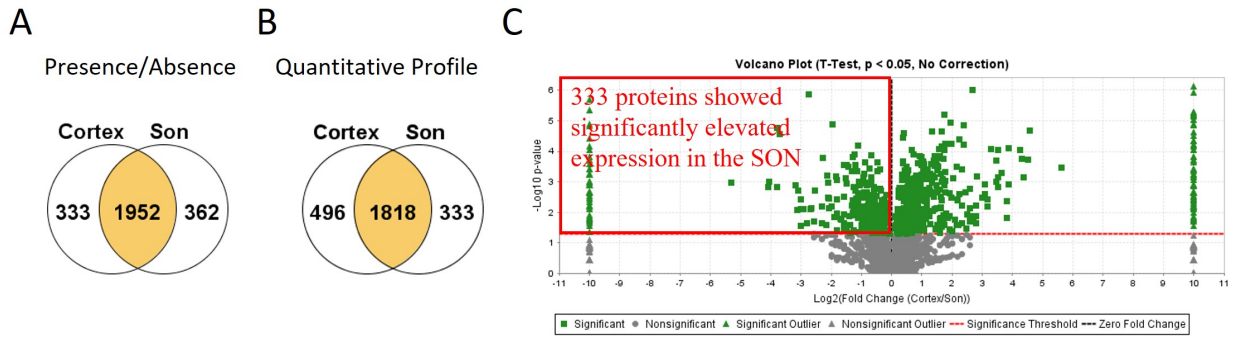

Figure 20. Comparative analysis of proteome from the SON and cortex using mass spectrometry.

A) 362 proteins are detected only in the SON; 333 proteins are detected only in the cortex; 1952 proteins are found in both brain areas. **B)** Following Student's t-test ($p < 0.05$), 333 proteins are elevated significantly in the SON compared to the cortex. **C)** Volcano plot displays the distribution of 2647 proteins detected in the SON and cortex. Green points on the left half represent proteins (333) that have significantly increased expression levels in the SON compared to the cortex. Green points on the right half represent proteins (496) that have significantly increased expression levels in the cortex compared to the SON. Grey points below the red dotted line represent proteins (1818) whose expression levels do not significantly change between the SON and cortex. SON (n = 3); cortex (n = 3).

4. Discussion

4.1 Actin cytoskeleton density increases in high dietary salt (HDS) rat models

Recent studies have shown that the density of actin is elevated in VP neurons in rats under SL [103]. Similarly, in our study, we found that rats chronically exposed to mildly elevated sodium chow display increased actin density in SON VP neurons. Although to various extents, salt-insensitive rats exposed to both HDS models that we mentioned above display elevated density of cortical actin layers and comet-like actin structures in the cytoplasm. Note that rat strains that are sensitive to salt developed by selective breeding, for example spontaneously hypertensive rats [218] and Dahl salt-sensitive rats [219]. However, we specifically focused on salt-insensitive rats because they are more physiologically relevant to the high salt consumption situation happening in humans, as most healthy young individuals do not develop hypertension under chronic high sodium food consumption. Thus, it is important to study the changes in the actin cytoskeleton following a more chronic HDS regiment (2 months instead of 7 days) without triggering plasma osmolality increase or BP elevation. Indeed, in rats fed elevated sodium chow model, we observed a significantly increased subcortical actin intensity in 2% and 4% NaCl chow fed rats even with a small sample size. However, no change was observed in the subcortical actin intensity between 2% and 4% NaCl chow fed rats. This may be due to other compensatory mechanisms playing a role in this long-term HDS treatment (2 months instead of 7 days), so 2% NaCl and 4% NaCl do not make a big difference. Although the thickness of the actin layer does not increase significantly in 2% or 4% NaCl chow fed rats, a trend to increase in 4% NaCl chow fed rats was observed. More animals should be analyzed to test this effect. Likewise, chronic exposure to 2% and 4% NaCl chow also significantly increased the comet-like actin structure density and length. Our results suggest that increased actin cytoskeleton density in

VP neurons is likely to be a consequence of HDS intake, and is not caused by the increased plasma osmolality and/or elevated BP.

Two hypotheses were raised to explain the increased density of actin filaments and MTs in VP neurons upon HDS. The first hypothesis implied that the increased density of actin filaments and MTs upon HDS is triggered by increased expression of actin and tubulin, which leads to the elevation of the concentration of actin and tubulin monomers, thus shifting the dynamics towards polymerization of new actin filaments and MTs. The second hypothesis suggests that the increased density of actin filaments and MTs is a result of HDS-induced activation of actin and/or MT polymerizing molecules, whereas the concentration of actin and tubulin monomers remains unchanged.

Our western blot results comparing β-actin and β3-tubulin expression levels in the SON between control and SL rats support the second hypothesis. We found that the expression levels of β3-tubulin and β-actin in the SON do not change following SL, which suggests that there is no increased synthesis of actin and tubulin monomers under SL. This may indicate that the increased density of actin filaments and MTs in VP neurons observed using immunohistochemistry, which preferentially detects polymers and not monomers, is due to the shifted balance to promote polymerization mediated by SL-induced activation of actin and/or MT polymerizing molecules, and the overall actin and tubulin levels stay the same.

However, one limitation with western blot is that our samples are comprised of not only VP neurons. A cuboid-shape of the SON tissue was homogenized and lysed, and thus includes VP neurons, OT neurons, glial cells, blood vessels, extracellular matrix, and possibly other cells outside the SON. Therefore, potential changes of actin expression in only VP neurons can be diluted in the whole tissue lysates. Nevertheless, given the ~2 fold increase in the density of actin

filaments and MTs in VP neurons [103,217] and the fact that 70% of the SON neuronal population comprises VP neurons [220], it is unlikely that we did not detect any changes in total protein levels using western blot, if this increased density would be due to elevated actin and tubulin expression levels.

4.2 Possible functions of the actin network in VP neurons

In vitro studies have shown that both monomeric tubulin and polymerized MTs can directly interact with TRPV1 channels via two highly conserved tubulin-binding domains on the C-terminus [108,109]. In addition, immunoprecipitation experiments and *in situ* proximity ligation assay proved that MTs interact with ΔN-TRPV1 channels directly in MNCs [106]. Unlike MTs, previous studies have indicated that actin does not bind directly to TRPV1 channels [104,105], which suggests that actin may regulate VP MNCs' activity indirectly. Two specialized actin structures have been found in VP neurons: a thin layer of actin filaments located beneath the plasma membrane and an array of comet-like actin structures in the cytoplasm [103].

Interestingly, the subcortical actin layer has been also found in other neuronal cell types (e.g., hippocampal CA1, CA3, dentate gyrus neurons, ARC, and parvocellular PVN neurons) [103]. However, the density and the thickness of the actin subcortical layer are the greatest in magnocellular VP neurons [103]. One hypothesis is that this actin subcortical layer provides mechanical support to VP neurons during osmotically-induced cell shrinking and push-activation, thus helping force transmission to mediate mechanical activation of ΔN-TRPV1 [103]. Indeed, a recent study by Levi et al. reported that SL increases cell stiffness in VP neurons [221]. An increase in VP neuron rigidity was not observed in rats subjected to another AngII-salt hypertension model which shows increased cytoplasmic alpha-tubulin but not subcortical actin

filaments [221]. This suggests that the mechanical support provided in the subcortical region might be mediated primarily by actin filaments. Previous studies have characterized that the intensity and the thickness of the subcortical actin layer increase dramatically after SL [103]. Similarly, we observed an increased subcortical actin layer intensity in 2% and 4% NaCl chow fed rats in the elevated sodium chow model. The thickness of the actin layer displays a trend to increase in 4% NaCl chow fed rats, and confirming this observation requires a larger sample size. In conclusion, *in situ* characterization of the subcortical actin layer in both models is consistent with the hypothesis that the subcortical actin layer provides mechanical support to the VP neurons. An increased actin density may contribute to the increased mechanosensitivity and osmosensitivity of VP neurons during chronic HDS, resulting in more VP release to restore body fluid homeostasis.

Unlike the subcortical actin layer that has been observed in several other neuronal cell types, the comet-like actin structures appear to be unique to MNCs [103]. Those structures have been proposed to be involved in organelle/vesicle trafficking since they resemble actin comet-like tails propelling the movement of bacteria *Listeria monocytogenes* within the cytoplasm of infected cells and filamentous actin structures propelling endosomes and endocytic vesicles [103]. It is conceivable that the comet-like actin structures are involved in the trafficking of VP secretory vesicles [103]. SL triggers an increase in both the density and the length of the comet-like actin structures in VP neurons [103]. Likewise, in the present study, chronic exposure to 2% and 4% NaCl chow increases the comet-like actin structure density and length, although to a smaller extent compared to SL. These results are consistent with our hypothesis that since more VP is released in chronic HDS, more comet-like actin structures are required to transport a larger

number of VP-containing secretory vesicles. Using live-cell imaging, future studies should explore the functions of these comet-like actin structures.

4.3 RhoA and mDia1 activation in VP neurons

Our hypothesis states that an increase in the density of actin filaments and MTs may mediate the increase in the mechanosensitivity and osmosensitivity of VP neurons in SL. A fundamental question is what molecular mechanisms are mediating the increase in actin and microtubule polymerization. Formins are involved in regulating both actin filaments and MTs in a variety of cell types [118]. mDia1, as the most well-studied member among mammalian formins, is enriched in the SON compared to other brain areas in the baseline condition (Figure 8). Moreover, mDia1 has been shown to increase beneath the plasma membrane of VP neurons in the SON and PVN following 7 days of SL (Figure 9).

Previous studies have shown that mDia1 is localized under the plasma membrane upon activation in cultured cells [162–164]. In this thesis, we observed that mDia1 levels are increased close to the surface of VP neurons upon SL, which suggests that mDia1 might be activated. Previous studies in our lab used two different mDia1 antibodies, one hosted in rabbit (rabbit anti-mDia1), and another hosted in mouse (mouse anti-mDia1). The increased mDia1 expression in the SON was observed using both antibodies, whereas enriched cortical levels of mDia1 were only found in the SON using rabbit anti-mDia1 antibody (Figure 9A-B), but not mouse anti-mDia1 (Figure 8A). Indeed, these two antibodies can recognize different amino acid sequences from mDia1 protein. The rabbit anti-mDia1 antibody binds to rat mDia1 amino acid sequence 1143-1265 (human mDia1 amino acid sequence 1158-1272) in the C-terminus, which overlaps with the catalytic FH2 domain (amino acid sequence 762-1164) and the DAD domain (amino acid sequence 1187-1215), while the mouse anti-mDia1 antibody binds to rat mDia1 amino acid

sequence 50-162 (mouse mDia1 amino acid sequence 41-153) in the N-terminus which overlaps with the GBD binding domain (amino acid sequence 84-499). In a non-activated/resting state, mDia1 is present in an autoinhibited conformation, mediated by DID-DAD interactions tentatively masking the catalytic domain thereby preventing its interaction with actin and tubulin to promote filament polymerization [132–136]. Accordingly, these DID-DAD interactions might also mask and make the C-terminus (FH1, FH2, and DAD domains) not accessible by the antibody when mDia1 is in the autoinhibited state. Thus, we hypothesized that the rabbit anti-mDia1 antibody may preferentially bind to the active mDia1 confirmation when C-terminus is not interacting with other domains. However, the mouse anti-mDia1 antibody that targets the N-terminus can potentially bind to both active and inactive mDia1 indiscriminately.

An additional rabbit anti-mDia1 antibody was used in this study. The new rabbit anti-mDia1 antibody targets rat mDia1 amino acid sequence 1204-1265 (human mDia1 amino acid sequence 1211-1272) in the C-terminus, which overlaps with the DAD domain (amino acid sequence 1187-1215). Enriched subcortical mDia1 expression in VP neurons stained by this antibody also suggests that antibodies targeting the C-terminus might specifically bind to an activate confirmation of mDia1.

In our study, RhoA cortical levels also increase in VP neurons following SL. RhoA has been reported to translocate to the plasma membrane upon activation in non-neuronal cells [165]. As one of the two major downstream effectors of RhoA, mDia1 has been found to be recruited to the plasma membrane upon activation *in vitro* [162–164]. Moreover, binding of RhoA to mDia1 causes dissociation of DAD peptides from DID-DAD autoinhibited interactions and activation of FH2-DAD proteins [222,223]. This supports that displacement of DAD from the N-terminus is

required by mDia1 activation by RhoA. Therefore, mDia1 might be recruited and activated by RhoA beneath the plasma membrane.

Furthermore, our western blot analysis suggests that total mDia1 and RhoA levels are not altered in the SON following SL. This indicates that the elevated mDia1 and RhoA expression levels caused by SL observed in immunohistochemistry results are caused by increased activation, but not by an overall higher expression of RhoA and mDia1. This hypothesis is consistent with the elevated cortical levels of mDia1 and RhoA in VP neurons following SL. However, cytoplasmic mDia1 levels also increase under SL while we did not observe increased cytoplasmic levels of RhoA. It is conceivable that active mDia1 is also present in the cytoplasm, or interacting with the vesicles or other membrane-containing organelles. Another possible explanation is that although the rabbit anti-mDia1 antibody used in this study preferably binds to active mDia1, it can also bind to inactive mDia1. But this relatively mild change was not detected by western blot since changes only in VP neurons can be diluted in whole tissue lysates of the SON.

RhoA activation in VP neurons upon SL will be further examined by pull-down assays for activated RhoA GTPases which have been used in brain tissue lysates before by Kramar et al. [215]. The assay uses the Rho binding domain (RBD) of the Rho effector protein, Rhotekin. The RBD motif has been shown to bind specifically to the activated GTP-bound form of RhoA [224]. Further work should also study if RhoA activation is sufficient to recapitulate the effects of SL on mDia1 and cytoskeleton reorganization by injecting adeno-associated viruses (AAVs) expressing Cre-dependent constitutively active RhoA (e.g., Rho-V14) into the SON of rats fed control diet.

4.4 Specificity of formin inhibitor SMIFH2

Upon icv injection of formin inhibitor SMIFH2, actin cytoskeleton density decreases in SON VP neurons in rats under SL. Thus, we hypothesized that formin activation may contribute to the increased polymerization of the actin cytoskeleton in SON VP neurons in SL. However, a major concern related to this experiment is that the specificity of SMIFH2 has been questioned.

First identified and characterized by Rizvi et al., SMIFH2 is a cell-permeable compound that inhibits Formin-dependent actin polymerization by targeting the FH2 domain [225]. A small-molecule screen was conducted to select the compounds that prevent the assembly of actin filaments mediated by the mouse formin mDia1 and mDia2 in the presence of profilin *in vitro*. Half-maximal inhibition of mDia1 occurs at ~15 μM SMIFH2 concentration. in the presence of saturating SMIFH2 concentrations, the actin assembly rate is identical to the actin assembly rate without formins. Moreover, SMIFH2 has been demonstrated to be specific to formin-mediated actin assembly, but not a spontaneous assembly of actin monomers without formins, the addition of actin to the barbed end of pre-assembled filaments without formins or actin polymerization stimulated with Arp2/3 complex. With IC50 ranging from 5–15 μM SMIFH2, formins from a variety of species (*C. elegans, S. pombe, S. cerevisae,* and *M. musculus*) are inhibited. This suggests that SMIFH2 may block the activity of all formins. However, this prediction has not been tested directly. As the only well-characterized and commercialized formin inhibitor, SMIFH2 is widely used in biology studies to investigate formin functions.

However, recent studies have found that the action of SMIFH2 may go beyond formin inhibition. The high electrophilic nature of SMIFH2 suggests that it can have nonspecific targets [226]. It has been reported that SMIFH2 can reduce the expression and activity of p53 through a post-transcriptional, proteasome-independent mechanism [227]. Since SMIFH2 also induces

cytotoxicity at high doses, the authors suggested that SMIFH2 should be employed with short incubation (< 1 hour) and moderate concentrations (< 25 μM) for *in vitro* study. Moreover, an additional off-target effect has been recently identified suggesting that SMIFH2 is a potent inhibitor of molecular motors of the myosin family [228]. SMIFH2 has been found to inhibit the activity of human non-muscle myosin 2A with an IC50 of ~50 μM. As a molecular motor, myosin mediates numerous cellular processes which require actin polymerization. In addition, SMIFH2 at concentrations ≥ 5–10 μM shows *in vivo* toxicity in developing zebrafish [229]. Thus, SMIFH2 should be carefully applied with appropriate concentration and treatment duration when probing formin functions.

Applied concentrations and treatment duration are highly variable through studies. SMIFH2 has been used at concentrations ranging from 5–100 μM and for incubation times of < 1 h to > 24 h [227]. The employed concentrations and incubation times have not been well defined in terms of the target specificity and toxicity of SMIFH2. In addition, SMIFH2 has not been employed in the nervous system *in vivo* before, so it is difficult to establish an appropriate concentration for the present study. The CSF volume in three-month-old rats is about 270 μl [230]. Based on that, in our experiment, the final concentrations of SMIFH2 in the CSF are approximately 110 μM (salt loaded for 7 days) and 220 μM (salt loaded for 5 days) at the point of injection. The turnover rate of CSF is 9-11 per day in rats between 3-20 months, which translates into a CSF secretion rate of 84 μl/h [230]. Although CSF turnover should be considered when we extrapolate SMIFH2 concentrations during the course of SL, it is likely that high concentrations of SMIFH2 would trigger unspecific effects in the brain. Unfortunately, other more specific formin inhibitors are not yet available.

More specific ways to investigate mDia1 functions include knocking down mDia1 selectively in VP neurons by injecting AAVs expressing Cre-dependent loxP-shRNA targeting mDia1 into the SON of VP-Cre rats or inhibiting mDia1 by injecting AAVs expressing a dominant-negative mDia1 fragment in a Cre-dependent manner.

4.5 Identification of cytoskeleton-related proteins enriched in the SON as compared to the cortex

In addition to mDia1, additional cytoskeleton-regulating proteins might also play a role in the regulation of unique cytoskeletal networks in VP neurons in the SON and PVN in normal physiological conditions as well as in response to acute or chronic osmotic stimuli.

DRFs that include mDia, Daam, FMNL, and FHOD mammalian formin families have been proved to dully regulate actin and MTs. They share a similar domain organization with the same autoinhibitory mechanism mediated by DID-DAD interactions [131]. Moreover, previous research implies that in addition to mDia1, mDia2 [231], and Daam1 [232,233] can also bind to RhoA [131]. Therefore, it is conceivable that other DRFs play a role in the cytoskeleton regulation in VP neurons. However, our mass spectrometry results suggest that only very low expression levels of mDia1 and Daam1 were detected in some of the samples, while other samples show no mDia1 or Daam1 expression. One possible explanation is that mass spectrometry is not sensitive to detect low abundance proteins. In summary, whether additional DRFs are involved in cytoskeleton regulation in VP neurons remains to be investigated.

Among 333 proteins that increase significantly in the SON, many cytoskeleton-related proteins were identified, for example, Myristoylated alanine-rich C-kinase substrate (Marcks), tubulin-binding protein Tubulin polymerization-promoting protein family member 3 (Tppp3), and Ena/VASP-like protein (Evl). Furthermore, four out of five isoforms of CRMP (collapsin-

response mediator protein) family were detected in both the rat SON and cortex. CRMP family consists of five intracellular phosphoproteins (CRMP1, CRMP2, CRMP3, CRMP4, CRMP5), which play important roles in neuronal differentiation, axonal growth, guidance, axon/dendrite specification [234]. Our data revealed that CRMP2, CRMP3, CRMP4, CRMP5 expression levels increase in the SON compared to cortex (CRMP2: 1.1 fold, $p = 0.0028$; CRMP3: 1.2 fold, $p = 0.023$; CRMP4: 1.4 fold, $p = 0.0076$; CRMP5: 1.6 fold, $p = 0.0007$). Moreover, previous studies have shown that CRMP4 can promote both MT assembly and actin filament bundling *in vitro.* In addition, CRMP4 is the sole CRMP isoform that can bind to RhoA [235]. Therefore, CRMP4 might contribute to the unique organization of cytoskeleton in the SON. Further work needs to be done to study the functions of the CRMP family in the SON.

Furthermore, proteins that were found to have lower expression levels in the SON compared to the cortex should be investigated as well. Potential cytoskeleton-related proteins will be identified as they might play an inhibitory role, and decreased expression of these in the SON might promote the polymerization of the actin filaments and/or MTs.

Conclusion

While the link between HDS and hypertension is well established [28,29], the molecular mechanisms underlying HDS-induced increases in BP remain unclear. Recent studies revealed that magnocellular VP neurons harbor unique cytoskeletal networks which are comprised of a thin layer of actin filaments beneath the plasma membrane, an array of comet-like actin structures within the cytoplasm, and a dense interweaved network of MTs that occupy the entire cytoplasm [103,217]. Notably, VP neuron excitability is proportional to the density of these cytoskeletons [99,106]. Furthermore, recent studies have shown that the density of actin and MTs are elevated in VP neurons in rats after SL [103,217].

This study aimed to elucidate the molecular mechanisms that can lead to the increased polymerization of actin and tubulin in VP neurons in SL. Our results suggest that the activation of RhoA-mDia1 signaling is increased in SL in VP neurons while the overall expression of RhoA-mDia1 is not changed. Furthermore, a decrease in the actin cytoskeleton density in SMIFH2-treated rats in SL suggests that formin activation may contribute to the increased polymerization of actin cytoskeleton in SON VP neurons during SL. In addition, by evaluating actin cytoskeleton density in rats chronically exposed to mildly elevated sodium chow, we hypothesized that the increased actin polymerization in SON VP neurons is triggered by HDS intake, and not a consequence of elevated plasma osmolality and high BP. To investigate additional molecular pathways that might be involved in regulating cytoskeletal structures in the SON and their reorganization in HDS, we used an unbiased approach to analyze the proteome of the rat SON and cortex, leading to the identification of additional cytoskeleton-regulating proteins, whose roles pending further investigation. Additional analysis of SON and cortex proteome to identify other cytoskeleton-related proteins may provide insights into the mechanisms underlying the maintenance of unique cytoskeletal structures in magnocellular VP neurons.

In conclusion, this study increases our understanding of fluid balance disorders by examining the mechanisms by which HDS leads to enhanced VP secretion, thus contributing to the development of hypertension. Moreover, the identification of the signaling molecules mediating the hyperactivity of VP neurons in HDS will contribute to the development of novel therapies for the resistant forms of hypertension.

References

1. Bourque CW: **Central mechanisms of osmosensation and systemic osmoregulation**. 2008, **9**.

2. Machino T, Yoshizawa T: **Brain shrinkage due to acute hypernatremia**. *Neurology* 2006, **67**:880.

3. Ayus JC, Varon J, Arieff AI: **Hyponatremia, cerebral edema, and noncardiogenic pulmonary edema in marathon runners**. *Ann Intern Med* 2000, **132**:711–714.

4. Saly V, Andrew RD: **CA3 neuron excitation and epileptiform discharge are sensitive to osmolality**. *J Neurophysiol* 1993, **69**:2200–2208.

5. Pasantes-Morales H, Tuz K: **Volume changes in neurons: hyperexcitability and neuronal death**. *Contrib Nephrol* 2006, **152**:221–240.

6. Swaab DF, Nijveldt F, Pool CW: **Distribution of oxytocin and vasopressin in the rat supraoptic and paraventricular nucleus**. *J Endocrinol* 1975, **67**:461–462.

7. Vandesande F, Dierickx K: **Identification of the vasopressin producing and of the oxytocin producing neurons in the hypothalamic magnocellular neurosecretroy system of the rat**. *Cell Tissue Res* 1975, **164**:153–162.

8. Olff M, Frijling JL, Kubzansky LD, Bradley B, Ellenbogen MA, Cardoso C, Bartz JA, Yee JR, van Zuiden M: **The role of oxytocin in social bonding, stress regulation and mental health: An update on the moderating effects of context and interindividual differences**. *Psychoneuroendocrinology* 2013, **38**:1883–1894.

9. Sherlock DA, Field PM, Raisman G: **Retrograde transport of horseradish peroxidase in the magnocellular neurosecretory system of the rat**. *Brain Res* 1975, **88**:403–414.

10. Bourque CW: **Activity-dependent modulation of nerve terminal excitation in a mammalian peptidergic system**. *Trends Neurosci* 1991, **14**:28–30.

11. Bicknell RJ: **Optimizing release from peptide hormone secretory nerve terminals**. *J Exp Biol* 1988, **139**:51–65.

12. Maghnie M: **Diabetes insipidus**. *Horm Res Paediatr* 2003, **59**:42–54.

13. Thibonnier M, Coles P, Thibonnier A, Shoham M: **Molecular pharmacology and modeling of vasopressin receptors**. *Prog Brain Res* 2002, **139**:179–196.

14. Mouillac B, Chini B, Balestre M-N, Elands J, Trumpp-Kallmeyer S, Hoflack J, Hibert M, Jard S, Barberis C: **The Binding Site of Neuropeptide Vasopressin V1a Receptor: EVIDENCE FOR A MAJOR LOCALIZATION WITHIN TRANSMEMBRANE REGIONS (*)**. *J Biol Chem* 1995, **270**:25771–25777.

15. Barberis C, Mouillac B, Durroux T: **Structural bases of vasopressin/oxytocin receptor function**. *J Endocrinol* 1998, **156**:223–229.

16. Bankir L, Bichet DG, Morgenthaler NG: **Vasopressin: physiology, assessment and osmosensation**. *J Intern Med* 2017, **282**:284–297.

17. Science B, Vasopressin L, Barlow M: **Vasopressin**. *Emerg Med* 2002, **14**:304–314.

18. Stanaway JD, Afshin A, Gakidou E, Lim SS, Abate D, Abate KH, Abbafati C, Abbasi N, Abbastabar H, Abd-Allah F, et al.: **Global, regional, and national comparative risk assessment of 84 behavioural, environmental and occupational, and metabolic risks or clusters of risks for 195 countries and territories, 1990–2017: a systematic analysis for the Global Burden of Disease Stu**. *Lancet* 2018, **392**:1923–1994.

19. Roth GA, Abate D, Abate KH, Abay SM, Abbafati C, Abbasi N, Abbastabar H, Abd-Allah F, Abdela J, Abdelalim A, et al.: **Global, regional, and national age-sex-specific mortality for 282 causes of death in 195 countries and territories, 1980–2017: a systematic analysis for the Global Burden of Disease Study 2017**. *Lancet* 2018, **392**:1736–1788.

20. Mills KT, Bundy JD, Kelly TN, Reed JE, Kearney PM, Reynolds K, Chen J, He J: **Global Disparities of Hypertension Prevalence and Control: A Systematic Analysis of Population-Based Studies From 90 Countries**. *Circulation* 2016, **134**:441–450.

21. Gillis EE, Sullivan JC: **Sex Differences in Hypertension: Recent Advances**. *Hypertens (Dallas, Tex 1979)* 2016, **68**:1322.

22. Mills KT, Stefanescu A, He J: **The global epidemiology of hypertension**. *Nat Rev Nephrol 2020 164* 2020, **16**:223–237.

23. Arima H, Barzi F, Chalmers J: **Mortality patterns in hypertension**. *J Hypertens* 2011, **29 Suppl 1**.

24. Denton D, Weisinger R, Mundy NI, Wickings EJ, Dixson A, Moisson P, Pingard AM, Shade R, Carey D, Ardaillou R, et al.: **The effect of increased salt intake on blood pressure of chimpanzees**. *Nat Med* 1995, **1**:1009–1016.

25. He FJ, MacGregor GA: **Effect of modest salt reduction on blood pressure: a meta-analysis of randomized trials. Implications for public health**. *J Hum Hypertens* 2002, **16**:761–770.

26. Mente A, O'Donnell MJ, Rangarajan S, McQueen MJ, Poirier P, Wielgosz A, Morrison H, Li W, Wang X, Di C, et al.: **Association of urinary sodium and potassium excretion with blood pressure**. *N Engl J Med* 2014, **371**:601–611.

27. **Intersalt: an international study of electrolyte excretion and blood pressure. Results for 24 hour urinary sodium and potassium excretion. Intersalt Cooperative Research Group**. *BMJ* 1988, **297**:319–328.

28. Strazzullo P, D'Elia L, Kandala NB, Cappuccio FP: **Salt intake, stroke, and cardiovascular disease: meta-analysis of prospective studies**. *BMJ* 2009, **339**:1296.

29. Weinberger MH: **Salt sensitivity of blood pressure in humans**. *Hypertens (Dallas, Tex 1979)* 1996, **27**:481–490.

30. He FJ, Li J, MacGregor GA: **Effect of longer term modest salt reduction on blood pressure: Cochrane systematic review and meta-analysis of randomised trials**. *BMJ* 2013, **346**.

31. Ambard L: **Causes de l'hypertension arterielle**. *Arch Gen Med* 1904, **1**:520–533.

32. Kempner W: **Treatment of hypertensive vascular disease with rice diet**. *Am J Med* 1948, **4**:545–577.

33. Rust P, Ekmekcioglu C: **Impact of Salt Intake on the Pathogenesis and Treatment of Hypertension**. 2016, doi:10.1007/5584.

34. De Leeuw PW, Kroon AA: **Salt and sensitivity**. *Hypertens (Dallas, Tex 1979)* 2013, **62**:461–462.

35. Luzardo L, Noboa O, Boggia J: **Mechanisms of Salt-Sensitive Hypertension**. *Curr Hypertens Rev* 2015, **11**:14–21.

36. Farquhar WB, Edwards DG, Jurkovitz CT, Weintraub WS: **Dietary Sodium and Health: More Than Just Blood Pressure**. *J Am Coll Cardiol* 2015, **65**:1042.

37. Sanada H, Jones JE, Jose PA: **Genetics of Salt-Sensitive Hypertension**. *Curr Hypertens Rep* 2011, **13**:55.

38. Luft FC, Miller JZ, Grim CE, Fineberg NS, Christian JC, Daugherty SA, Weinberger MH: **Salt sensitivity and resistance of blood pressure. Age and race as factors in physiological responses**. *Hypertens (Dallas, Tex 1979)* 1991, **17**.

39. Chobanian A V., Bakris GL, Black HR, Cushman WC, Green LA, Izzo JL, Jones DW, Materson BJ, Oparil S, Wright JT, et al.: **Seventh report of the Joint National Committee on Prevention, Detection, Evaluation, and Treatment of High Blood Pressure**. *Hypertens (Dallas, Tex 1979)* 2003, **42**:1206–1252.

40. Robinson AT, Edwards DG, Farquhar WB: **The Influence of Dietary Salt Beyond Blood Pressure**. *Curr Hypertens Rep* 2019, **21**.

41. Farquhar WB, Edwards DG, Jurkovitz CT, Weintraub WS: **Dietary Sodium and Health: More Than Just Blood Pressure**. *J Am Coll Cardiol* 2015, **65**:1042.

42. Adler AJ, Taylor F, Martin N, Gottlieb S, Taylor RS, Ebrahim S: **Reduced dietary salt for the prevention of cardiovascular disease**. *Cochrane database Syst Rev* 2014, **2014**.

43. Graudal NA, Hubeck-Graudal T, Jurgens G: **Effects of low sodium diet versus high sodium diet on blood pressure, renin, aldosterone, catecholamines, cholesterol, and triglyceride**. *Cochrane database Syst Rev* 2017, **4**.

44. Graudal NA, Galløe AM, Garred P: **Effects of sodium restriction on blood pressure, renin, aldosterone, catecholamines, cholesterols, and triglyceride: a meta-analysis**. *JAMA* 1998, **279**:1383–1391.

45. Rivera SL, Martin J, Landry J: **Acute and Chronic Hypertension: What Clinicians Need to Know for Diagnosis and Management**. *Crit Care Nurs Clin North Am* 2019, **31**:97–108.

46. Zhao (D, Qi Y, Zheng Z, Wang Y, Zhang XY, Li HJ, Liu HH, Zhang XT, Du J, Liu J, et al.: **Dietary factors associated with hypertension**. *Nat Rev Cardiol 2011 88* 2011, **8**:456–465.

47. Porth CM: **Disorders of blood pressure regulation**. *Porth's Pathophysiol Lippincott* 2009,

48. Voisin DL, Bourque CW: **Integration of sodium and osmosensory signals in vasopressin neurons**. *Trends Neurosci* 2002, **25**:199–205.

49. Bourque CW: **Central mechanisms of osmosensation and systemic osmoregulation**. *Nat Rev Neurosci* 2008, **9**:519–531.

50. Robertson GL, Shelton RL, Athar S: **The osmoregulation of vasopressin**. *Kidney Int* 1976, **10**:25–37.

51. Dunn FL, Brennan TJ, Nelson AE, Robertson GL: **The role of blood osmolality and volume in regulating vasopressin secretion in the rat**. *J Clin Invest* 1973, **52**:3212–3219.

52. de Wardener HE, He FJ, MacGregor GA: **Plasma sodium and hypertension**. *Kidney Int* 2004, **66**:2454–2466.

53. Ludwig M, Williams K, Callahan MF, Morris M: **Salt loading abolishes osmotically stimulated vasopressin release within the supraoptic nucleus**. *Neurosci Lett* 1996, **215**:1–4.

54. Danziger J, Zeidel ML: **Osmotic homeostasis**. *Clin J Am Soc Nephrol* 2015, **10**:852–862.

55. Hinojosa C, Shade RE, Haywood JR: **Plasma vasopressin concentration in high sodium renal hypertension**. *J Hypertens* 1986, **4**:529–534.

56. Dipette DJ, Gavras I, North WG, Brunner HR, Gavras H: **Vasopressin in salt-induced hypertension of experimental renal insufficiency**. *Hypertens (Dallas, Tex 1979)* 1982, **4**:125–130.

57. Crofton JT, Share L, Shade RE, Lee-Kwon WJ, Manning M, Sawyer WH: **The importance of vasopressin in the development and maintenance of DOC-salt hypertension in the rat**. *Hypertens (Dallas, Tex 1979)* 1979, **1**:31–38.

58. Henderson KK, Byron KL: **Vasopressin-induced vasoconstriction: two concentration-dependent signaling pathways**. *J Appl Physiol* 2007, **102**:1402–1409.

59. Postma CT, Maessen SMJ, Thien TH, Smits P: **The effect of arginine vasopressin on endothelin production in the human forearm vascular bed**. *Neth J Med* 2005, **63**:199–204.

60. Kutina A V., Marina AS, Natochin Y V.: **A novel natriuretic factor in hypervolemia**. *Dokl Biol Sci Proc Acad Sci USSR, Biol Sci Sect* 2011, **441**:360–362.

61. Hür E, Özişik M, Ural C, Yildiz G, Małden K, Köse SB, Köktürk F, Büyükuysal Ç, Yildirim I, Süleymanlar G, et al.: **Hypervolemia for Hypertension Pathophysiology: A Population-Based Study**. *Biomed Res Int* 2014, **2014**.

62. Bauer JH, Brooks CS: **Volume studies in men with mild to moderate hypertension**. *Am J Cardiol* 1979, **44**:1163–1170.

63. Garay RP, Dagher G, Meyer P: **An inherited sodium ion-potassium ion cotransport defect in essential hypertension**. *Clin Sci (Lond)* 1980, **59 Suppl 6**.

64. Ibsen H, Leth A: **Plasma volume and extracellular fluid volume in essential hypertension**. *Acta Med Scand* 1973, **1**–**2**:93–96.

65. Bauer JH, Brooks CS: **Body-fluid composition in normal and hypertensive man**. *Clin Sci (Lond)* 1982, **62**:43–49.

66. Fountain JH, Lappin SL: **Physiology, renin angiotensin system**. 2017,

67. Herman LL, Padala SA, Ahmed I, Bashir K: **Angiotensin Converting Enzyme Inhibitors (ACEI)**. 2022,

68. Bie P, Evans RG: **Normotension, hypertension and body fluid regulation: brain and kidney**. *Acta Physiol (Oxf)* 2017, **219**:288–304.

69. Veerasingham SJ, Raizada MK: **Brain renin-angiotensin system dysfunction in hypertension: recent advances and perspectives**. *Br J Pharmacol* 2003, **139**:191–202.

70. Farquhar WB, Edwards DG, Jurkovitz CT, Weintraub WS: **Dietary sodium and health: more than just blood pressure**. *J Am Coll Cardiol* 2015, **65**:1042–1050.

71. Rimoldi SF, Messerli FH, Bangalore S, Scherrer U: **Resistant hypertension: what the cardiologist needs to know**. *Eur Heart J* 2015, **36**:2686-2695c.

72. Te Riet L, Van Esch JHM, Roks AJM, Van Den Meiracker AH, Danser AHJ: **Hypertension: renin-angiotensin-aldosterone system alterations**. *Circ Res* 2015, **116**:960–975.

73. Choe KY, Han SY, Gaub P, Shell B, Voisin DL, Blayne A, Barker PA, Brown CH, Cunningham JT, Charles W: **High Salt Intake Increases Blood Pressure via BDNF-Mediated Downregulation of KCC2 and Impaired Baroreflex Inhibition of Vasopressin Neurons**. 2015, **85**:549–560.

74. Kim YB, Kim YS, Kim W Bin, Shen FY, Lee SW, Chung HJ, Kim JS, Han HC, Colwell CS, Kim YI: **GABAergic excitation of vasopressin neurons: possible mechanism underlying sodium-dependent hypertension**. *Circ Res* 2013, **113**:1296–1307.

75. Kim JS, Kim W Bin, Kim YB, Lee Y, Kim YS, Shen FY, Lee SW, Park D, Choi HJ, Hur J, et al.: **Chronic hyperosmotic stress converts GABAergic inhibition into excitation in vasopressin and oxytocin neurons in the rat**. *J Neurosci* 2011, **31**:13312–13322.

76. Antoni FA: **Vasopressin as a stress hormone**. *Stress Neuroendocrinol Neurobiol Handb Stress Ser Vol 2* 2016, **2**:97.

77. Bourque CW, Oliet SHR, Richard D: **Osmoreceptors, osmoreception, and osmoregulation**. *Front Neuroendocrinol* 1994, **15**:231–274.

78. Bourque CW: **Central mechanisms of osmosensation and systemic osmoregulation**. *Nat Rev Neurosci* 2008, **9**:519–531.

79. Armstrong WE, Tian M, Wong H: **Electron microscopic analysis of synaptic inputs**

from the median preoptic nucleus and adjacent regions to the supraoptic nucleus in the rat. *J Comp Neurol* 1996, **373**:228–239.

80. Stachniak TJ, Trudel E, Bourque CW: **Cell-specific retrograde signals mediate antiparallel effects of angiotensin II on osmoreceptor afferents to vasopressin and oxytocin neurons**. *Cell Rep* 2014, **8**:355–362.

81. Leng G, Blackburn RE, Dyball REJ, Russell JA: **Role of anterior peri-third ventricular structures in the regulation of supraoptic neuronal activity and neurohypophysical hormone secretion in the rat**. *J Neuroendocrinol* 1989, **1**:35–46.

82. Richard D, Bourque CW: **Synaptic control of rat supraoptic neurones during osmotic stimulation of the organum vasculosum lamina terminalis in vitro**. *J Physiol* 1995, **489 (Pt 2**:567–577.

83. Ciura S, Bourque CW: **Transient receptor potential vanilloid 1 is required for intrinsic osmoreception in organum vasculosum lamina terminalis neurons and for normal thirst responses to systemic hyperosmolality**. *J Neurosci* 2006, **26**:9069–9075.

84. Ciura S, Liedtke W, Bourque CW: **Hypertonicity sensing in organum vasculosum lamina terminalis neurons: a mechanical process involving TRPV1 but not TRPV4**. *J Neurosci* 2011, **31**:14669–14676.

85. Choe KY, Olson JE, Bourque CW: **Taurine release by astrocytes modulates osmosensitive glycine receptor tone and excitability in the adult supraoptic nucleus**. *J Neurosci* 2012, **32**:12518–12527.

86. Deleuze C, Duvoid A, Hussy N: **Properties and glial origin of osmotic-dependent release of taurine from the rat supraoptic nucleus**. *J Physiol* 1998, **507 (Pt 2**:463–471.

87. Hussy N, Deleuze C, Pantaloni A, Desarménien MG, Moos F: **Agonist action of taurine on glycine receptors in rat supraoptic magnocellular neurones: possible role in osmoregulation**. *J Physiol* 1997, **502 (Pt 3**:609–621.

88. Bourque CW: **Ionic basis for the intrinsic activation of rat supraoptic neurones by hyperosmotic stimuli**. *J Physiol* 1989, **417**:263–277.

89. Oliet SHR, Bourque CW: **Steady-state osmotic modulation of cationic conductance in neurons of rat supraoptic nucleus**. *Am J Physiol* 1993, **265**.

90. Oliet SHR, Bourque C: **Mechanosensitive channels transduce osmosensitivity in supraoptic neurons**. *Nature* 1993, **364**:341–343.

91. Lang F: **Mechanisms and significance of cell volume regulation**. *J Am Coll Nutr* 2007, **26**:613S-623S.

92. Strange K: **Cellular volume homeostasis**. *Adv Physiol Educ* 2004, **28**:155–159.

93. Zhang Z, Bourque CW: **Osmometry in osmosensory neurons**. *Nat Neurosci* 2003, **6**:1021–1022.

94. Prager-Khoutorsky M: **Mechanosensing in hypothalamic osmosensory neurons**. *Semin Cell Dev Biol* 2017, **71**:13–21.

95. Zhang Z, Kindrat AN, Sharif-Naeini R, Bourque CW: **Actin filaments mediate mechanical gating during osmosensory transduction in rat supraoptic nucleus neurons**. *J Neurosci* 2007, **27**:4008–4013.

96. Naeini RS, Witty MF, Séguéla P, Bourque CW: **An N-terminal variant of Trpv1 channel is required for osmosensory transduction**. *Nat Neurosci* 2006, **9**:93–98.

97. Zaelzer C, Hua P, Prager-Khoutorsky M, Ciura S, Voisin DL, Liedtke W, Bourque CW: **ΔN-TRPV1: A Molecular Co-detector of Body Temperature and Osmotic Stress**. *Cell Rep* 2015, **13**:23–30.

98. Zhang Z, Kindrat AN, Sharif-Naeini R, Bourque CW: **Actin filaments mediate mechanical gating during osmosensory transduction in rat supraoptic nucleus neurons**. *J Neurosci* 2007, **27**:4008–4013.

99. Zhang Z, Bourque CW: **Amplification of transducer gain by angiotensin II-mediated enhancement of cortical actin density in osmosensory neurons**. *J Neurosci* 2008, **28**:9536–9544.

100. Ishibashi S, Oomura Y, Gueguen B, Nicolaidis S: **Neuronal responses in subfornical organ and other regions to angiotensin II applied by various routes**. *Brain Res Bull* 1985, **14**:307–313.

101. Potts PD, Ludbrook J, Gillman-Gaspari TA, Horiuchi J, Dampney RAL: **Activation of brain neurons following central hypervolaemia and hypovolaemia: contribution of baroreceptor and non-baroreceptor inputs**. *Neuroscience* 2000, **95**:499–511.

102. Nicolaidis S, Ishibashi S, Gueguen B, Thornton SN, de Beaurepaire R: **Iontophoretic investigation of identified SFO angiotensin responsive neurons firing in relation to blood pressure changes**. *Brain Res Bull* 1983, **10**:357–363.

103. Barad Z, Jacob-Tomas S, Sobrero A, Lean G, Hicks AI, Yang J, Choe KY, Prager-Khoutorsky M: **Unique organization of actin cytoskeleton in magnocellular vasopressin neurons in normal conditions and in response to salt-loading**. *eNeuro* 2020, **7**:1–13.

104. Goswami C, Dreger M, Jahnel R, Bogen O, Gillen C, Hucho F: **Identification and characterization of a Ca2+ -sensitive interaction of the vanilloid receptor TRPV1 with tubulin**. *J Neurochem* 2004, **91**:1092–1103.

105. Goswami C, Hucho T: **Submembraneous microtubule cytoskeleton: biochemical and functional interplay of TRP channels with the cytoskeleton**. *FEBS J* 2008, **275**:4684–4699.

106. Prager-Khoutorsky M, Khoutorsky A, Bourque CW: **Unique Interweaved Microtubule Scaffold Mediates Osmosensory Transduction via Physical Interaction with TRPV1**. *Neuron* 2014, **83**:866–878.

107. Id MPO: **Effects of Salt Loading on the Organization of Microtubules in Rat Magnocellular Vasopressin Neurons**. 2020, doi:10.1111/jne.12817.

108. Goswami C, Hucho TB, Hucho F: **Identification and characterisation of novel tubulin-**

binding motifs located within the C-terminus of TRPV1. *J Neurochem* 2007, **101**:250–262.

109. Goswami C, Dreger M, Jahnel R, Bogen O, Gillen C, Hucho F: **Identification and characterization of a Ca 2+-sensitive interaction of the vanilloid receptor TRPV1 with tubulin**. *J Neurochem* 2004, **91**:1092–1103.

110. Hohmann T, Dehghani F: **The Cytoskeleton—A Complex Interacting Meshwork**. *Cells* 2019, **8**:362.

111. Sept D, Xu J, Pollard TD, McCammon JA: **Annealing accounts for the length of actin filaments formed by spontaneous polymerization.** *Biophys J* 1999, **77**:2911.

112. Sept D, Elcock AH, McCammon JA: **Computer simulations of actin polymerization can explain the barbed-pointed end asymmetry**. *J Mol Biol* 1999, **294**:1181–1189.

113. Pollard TD: **Actin and Actin-Binding Proteins**. *Cold Spring Harb Perspect Biol* 2016, **8**.

114. Weston L, Coutts AS, La Thangué NB: **Actin nucleators in the nucleus: an emerging theme**. *J Cell Sci* 2012, **125**:3519.

115. Sagot I, Rodal AA, Moseley J, Goode BL, Pellman D: **An actin nucleation mechanism mediated by Bni1 and profilin**. *Nat Cell Biol* 2002, **4**:626–631.

116. Pruyne D, Evangelista M, Yang C, Bi E, Zigmond S, Bretscher A, Boone C: **Role of formins in actin assembly: nucleation and barbed-end association**. *Science* 2002, **297**:612–615.

117. Roostalu J, Surrey T: **Microtubule nucleation: beyond the template**. *Nat Rev Mol Cell Biol* 2017, **18**:702–710.

118. Breitsprecher D, Goode BL: **Formins at a glance**. *J Cell Sci* 2013, **126**:1–7.

119. van Gisbergen PAC, Bezanilla M: **Plant formins: membrane anchors for actin polymerization**. *Trends Cell Biol* 2013, **23**:227–233.

120. Schönichen A, Geyer M: **Fifteen formins for an actin filament: a molecular view on the regulation of human formins**. *Biochim Biophys Acta* 2010, **1803**:152–163.

121. Kovar DR, Harris ES, Mahaffy R, Higgs HN, Pollard TD: **Control of the assembly of ATP- and ADP-actin by formins and profilin**. *Cell* 2006, **124**:423–435.

122. Romero S, Le Clainche C, Didry D, Egile C, Pantaloni D, Carlier MF: **Formin is a processive motor that requires profilin to accelerate actin assembly and associated ATP hydrolysis**. *Cell* 2004, **119**:419–429.

123. Vidali L, Van Gisbergen PAC, Guérin C, Franco P, Li M, Burkart GM, Augustine RC, Blanchoin L, Bezanilla M: **Rapid formin-mediated actin-filament elongation is essential for polarized plant cell growth**. *Proc Natl Acad Sci U S A* 2009, **106**:13341.

124. Schönichen A, Mannherz HG, Behrmann E, Mazur AJ, Kühn S, Silván U, Schoenenberger CA, Fackler OT, Raunser S, Dehmelt L, et al.: **FHOD1 is a combined actin filament capping and bundling factor that selectively associates with actin arcs**

and stress fibers. *J Cell Sci* 2013, **126**:1891–1901.

125. Michelot A, Derivery E, Paterski-Boujemaa R, Guérin C, Huang S, Parcy F, Staiger CJ, Blanchoin L: **A novel mechanism for the formation of actin-filament bundles by a nonprocessive formin**. *Curr Biol* 2006, **16**:1924–1930.

126. Harris ES, Rouiller I, Hanein D, Higgs HN: **Mechanistic differences in actin bundling activity of two mammalian formins, FRL1 and mDia2**. *J Biol Chem* 2006, **281**:14383–14392.

127. Gaillard J, Ramabhadran V, Neumanne E, Gurel P, Blanchoin L, Vantard M, Higgs HN: **Differential interactions of the formins INF2, mDia1, and mDia2 with microtubules**. *Mol Biol Cell* 2011, **22**:4575–4587.

128. Bartolini F, Moseley JB, Schmoranzer J, Cassimeris L, Goode BL, Gundersen GG: **The formin mDia2 stabilizes microtubules independently of its actin nucleation activity**. *J Cell Biol* 2008, **181**:523–536.

129. Wen Y, Eng CH, Schmoranzer J, Cabrera-Poch N, Morris EJS, Chen M, Wallar BJ, Alberts AS, Gundersen GG: **EB1 and APC bind to mDia to stabilize microtubules downstream of Rho and promote cell migration**. *Nat Cell Biol* 2004, **6**:820–830.

130. Thurston SF, Kulacz WA, Shaikh S, Lee JM, Copeland JW: **The ability to induce microtubule acetylation is a general feature of formin proteins**. *PLoS One* 2012, **7**.

131. Kühn S, Geyer M: **Formins as effector proteins of rho GTPases**. *Small GTPases* 2014, **5**:1–16.

132. Rose R, Weyand M, Lammers M, Ishizaki T, Ahmadian MR, Wittinghofer A: **Structural and mechanistic insights into the interaction between Rho and mammalian Dia**. *Nature* 2005, **435**:513–518.

133. Otomo T, Otomo C, Tomchick DR, Machius M, Rosen MK: **Structural basis of Rho GTPase-mediated activation of the formin mDia1**. *Mol Cell* 2005, **18**:273–281.

134. Li F, Higgs HN: **The mouse Formin mDia1 is a potent actin nucleation factor regulated by autoinhibition**. *Curr Biol* 2003, **13**:1335–1340.

135. Alberts AS: **Identification of a carboxyl-terminal diaphanous-related formin homology protein autoregulatory domain**. *J Biol Chem* 2001, **276**:2824–2830.

136. Otomo T, Tomchick DR, Otomo C, Machius M, Rosen MK: **Crystal structure of the Formin mDia1 in autoinhibited conformation**. *PLoS One* 2010, **5**:1–13.

137. Maiti S, Michelot A, Gould C, Blanchoin L, Sokolova O, Goode BL: **Structure and activity of full-length formin mDia1**. *Cytoskeleton (Hoboken)* 2012, **69**:393–405.

138. Nezami A, Poy F, Toms A, Zheng W, Eck MJ: **Crystal structure of a complex between amino and carboxy terminal fragments of mDia1: insights into autoinhibition of diaphanous-related formins**. *PLoS One* 2010, **5**:1–11.

139. Watanabe N, Madaule P, Reid T, Ishizaki T, Watanabe G, Kakizuka A, Saito Y, Nakao K, Jockusch BM, Narumiya S: **p140mDia, a mammalian homolog of Drosophila**

diaphanous, is a target protein for Rho small GTPase and is a ligand for profilin. *EMBO J* 1997, **16**:3044–3056.

140. Ridley AJ, Paterson HF, Johnston CL, Diekmann D, Hall A: **The small GTP-binding protein rac regulates growth factor-induced membrane ruffling**. *Cell* 1992, **70**:401–410.

141. R K, S A, A B, L L: **The Ras-related protein Cdc42Hs and bradykinin promote formation of peripheral actin microspikes and filopodia in Swiss 3T3 fibroblasts**. *Mol Cell Biol* 1995, **15**:1942–1952.

142. Nobes CD, Hall A: **Rho, rac, and cdc42 GTPases regulate the assembly of multimolecular focal complexes associated with actin stress fibers, lamellipodia, and filopodia**. *Cell* 1995, **81**:53–62.

143. Machesky LM, Insall RH: **Scar1 and the related Wiskott-Aldrich syndrome protein, WASP, regulate the actin cytoskeleton through the Arp2/3 complex**. *Curr Biol* 1998, **8**:1347–1356.

144. Rohatgi R, Ma L, Miki H, Lopez M, Kirchhausen T, Takenawa T, Kirschner MW: **The interaction between N-WASP and the Arp2/3 complex links Cdc42-dependent signals to actin assembly**. *Cell* 1999, **97**:221–231.

145. Ridley AJ, Hall A: **The small GTP-binding protein rho regulates the assembly of focal adhesions and actin stress fibers in response to growth factors**. *Cell* 1992, **70**:389–399.

146. Jaffe AB, Hall A: **Rho GTPases: biochemistry and biology**. *Annu Rev Cell Dev Biol* 2005, **21**:247–269.

147. Burridge K, Wennerberg K: **Rho and Rac take center stage**. *Cell* 2004, **116**:167–179.

148. Zheng Y: **Dbl family guanine nucleotide exchange factors**. *Trends Biochem Sci* 2001, **26**:724–732.

149. Moon SY, Zheng Y: **Rho GTPase-activating proteins in cell regulation**. *Trends Cell Biol* 2003, **13**:13–22.

150. Narumiya S, Tanji M, Ishizaki T: **Rho signaling, ROCK and mDia1, in transformation, metastasis and invasion**. *Cancer Metastasis Rev* 2009, **28**:65–76.

151. Yu M, Yuan X, Lu C, Le S, Kawamura R, Efremov AK, Zhao Z, Kozlov MM, Sheetz M, Bershadsky A, et al.: **MDia1 senses both force and torque during F-actin filament polymerization**. *Nat Commun* 2017, **8**.

152. Jégou A, Carlier MF, Romet-Lemonne G: **Formin mDia1 senses and generates mechanical forces on actin filaments**. *Nat Commun* 2013, **4**.

153. Gaillard J, Ramabhadran V, Neumanne E, Gurel P, Blanchoin L, Vantard M, Higgs HN: **Differential interactions of the formins INF2, mDia1,and mDia2 with microtubules**. *Mol Biol Cell* 2011, **22**:4575–4587.

154. Wen Y, Eng CH, Schmoranzer J, Cabrera-Poch N, Morris EJS, Chen M, Wallar BJ, Alberts AS, Gundersen GG: **EB1 and APC bind to mDia to stabilize microtubules**

downstream of Rho and promote cell migration. *Nat Cell Biol* 2004, **6**:820–830.

155. Lewkowicz E, Herit F, Clainche C Le, Bourdoncle P, Perez F, Niedergang F: **The microtubule-binding protein CLIP-170 coordinates mDia1 and actin reorganization during CR3-mediated phagocytosis**. *J Cell Biol* 2008, **183**:1287–1298.

156. Palazzo AF, Cook TA, Alberts AS, Gundersen GG: **mDia mediates Rho-regulated formation and orientation of stable microtubules**. *Nat Cell Biol* 2001, **3**:723–729.

157. Ishizaki T, Morishima Y, Okamoto M, Furuyashiki T, Kato T, Narumiya S: **Coordination of microtubules and the actin cytoskeleton by the Rho effector mDia1**. *Nat Cell Biol* 2001, **3**:8–14.

158. Goulimari P, Kitzing TM, Knieling H, Brandt DT, Offermanns S, Grosse R: **Galpha12/13 is essential for directed cell migration and localized Rho-Dia1 function**. *J Biol Chem* 2005, **280**:42242–42251.

159. Eng CH, Huckaba TM, Gundersen GG: **The formin mDia regulates GSK3beta through novel PKCs to promote microtubule stabilization but not MTOC reorientation in migrating fibroblasts**. *Mol Biol Cell* 2006, **17**:5004–5016.

160. Yamana N, Arakawa Y, Nishino T, Kurokawa K, Tanji M, Itoh RE, Monypenny J, Ishizaki T, Bito H, Nozaki K, et al.: **The Rho-mDia1 pathway regulates cell polarity and focal adhesion turnover in migrating cells through mobilizing Apc and c-Src**. *Mol Cell Biol* 2006, **26**:6844–6858.

161. Kodama A, Karakesisoglou I, Wong E, Vaezi A, Fuchs E: **ACF7: an essential integrator of microtubule dynamics**. *Cell* 2003, **115**:343–354.

162. Carramusa L, Ballestrem C, Zilberman Y, Bershadsky AD: **Mammalian diaphanous-related formin Dia1 controls the organization of E-cadherin-mediated cell-cell junctions**. *J Cell Sci* 2007, **120**:3870–3882.

163. Seth A, Otomo C, Rosen MK: **Autoinhibition regulates cellular localization and actin assembly activity of the diaphanous-related formins FRLα and mDia1**. *J Cell Biol* 2006, **174**:701–713.

164. Ramalingam N, Zhao H, Breitsprecher D, Lappalainen P, Faix J, Schleicher M: **Phospholipids regulate localization and activity of mDia1 formin**. *Eur J Cell Biol* 2010, **89**:723–732.

165. Van Unen J, Reinhard NR, Yin T, Wu YI, Postma M, Gadella TWJ, Goedhart J: **Plasma membrane restricted RhoGEF activity is sufficient for RhoA-mediated actin polymerization**. *Sci Rep* 2015, **5**.

166. De Conto F, Fazzi A, Razin S V., Arcangeletti MC, Medici MC, Belletti S, Chezzi C, Calderaro A: **Mammalian Diaphanous-related formin-1 restricts early phases of influenza A/NWS/33 virus (H1N1) infection in LLC-MK2 cells by affecting cytoskeleton dynamics**. *Mol Cell Biochem* 2018, **437**:185–201.

167. Gorelik R, Yang C, Kameswaran V, Dominguez R, Svitkina T: **Mechanisms of plasma membrane targeting of formin mDia2 through its amino terminal domains**. *Mol Biol*

Cell 2011, **22**:189–201.

168. Boyer O, Nevo F, Plaisier E, Funalot B, Gribouval O, Benoit G, Cong EH, Arrondel C, Tête M-J, Montjean R, et al.: **INF2 mutations in Charcot-Marie-Tooth disease with glomerulopathy**. *N Engl J Med* 2011, **365**:2377–2388.

169. Mademan I, Deconinck T, Dinopoulos A, Voit T, Schara U, Devriendt K, Meijers B, Lerut E, Jonghe P De, Baets J: **De novo INF2 mutations expand the genetic spectrum of hereditary neuropathy with glomerulopathy**. *Neurology* 2013, **81**:1953–1958.

170. Toyota K, Ogino D, Hayashi M, Taki M, Saito K, Abe A, Hashimoto T, Umetsu K, Tsukaguchi H, Hayasaka K: **INF2 mutations in Charcot-Marie-Tooth disease complicated with focal segmental glomerulosclerosis**. *J Peripher Nerv Syst* 2013, **18**:97–98.

171. Lybæk H, Ørstavik KH, Prescott T, Hovland R, Breilid H, Stansberg C, Steen VM, Houge G: **An 8.9 Mb 19p13 duplication associated with precocious puberty and a sporadic 3.9 Mb 2q23.3q24.1 deletion containing NR4A2 in mentally retarded members of a family with an intrachromosomal 19p-into-19q between-arm insertion**. *Eur J Hum Genet* 2009, **17**:904–910.

172. Law R, Dixon-Salazar T, Jerber J, Cai N, Abbasi AA, Zaki MS, Mittal K, Gabriel SB, Rafiq MA, Khan V, et al.: **Biallelic truncating mutations in FMN2, encoding the actin-regulatory protein Formin 2, cause nonsyndromic autosomal-recessive intellectual disability**. *Am J Hum Genet* 2014, **95**:721–728.

173. Cui Q, Xie P: **Correlation Between Daam2 Expression Changes and Demyelination in Guillain-Barre Syndrome**. *Cell Mol Neurobiol* 2016, **36**:683–688.

174. Ercan-Sencicek AG, Jambi S, Franjic D, Nishimura S, Li M, El-Fishawy P, Morgan TM, Sanders SJ, Bilguvar K, Suri M, et al.: **Homozygous loss of DIAPH1 is a novel cause of microcephaly in humans**. *Eur J Hum Genet* 2015, **23**:165–172.

175. Schymick JC, Scholz SW, Fung HC, Britton A, Arepalli S, Gibbs JR, Lombardo F, Matarin M, Kasperaviciute D, Hernandez DG, et al.: **Genome-wide genotyping in amyotrophic lateral sclerosis and neurologically normal controls: first stage analysis and public release of data**. *Lancet Neurol* 2007, **6**:322–328.

176. Proitsi P, Li T, Hamilton G, Di Forti M, Collier D, Killick R, Chen R, Sham P, Murray R, Powell J, et al.: **Positional pathway screen of wnt signaling genes in schizophrenia: association with DKK4**. *Biol Psychiatry* 2008, **63**:13–16.

177. Kuzman MR, Medved V, Terzic J, Krainc D: **Genome-wide expression analysis of peripheral blood identifies candidate biomarkers for schizophrenia**. *J Psychiatr Res* 2009, **43**:1073–1077.

178. Cappi C, Hounie AG, Mariani DB, Diniz JB, Silva ART, Reis VNS, Busso AF, Silva AG, Fidalgo F, Rogatto SR, et al.: **An inherited small microdeletion at 15q13.3 in a patient with early-onset obsessive-compulsive disorder**. *PLoS One* 2014, **9**.

179. Al-Maawali A, Barry BJ, Rajab A, El-Quessny M, Seman A, Coury SN, Barkovich AJ, Yang E, Walsh CA, Mochida GH, et al.: **Novel loss-of-function variants in DIAPH1**

associated with syndromic microcephaly, blindness, and early onset seizures. *Am J Med Genet A* 2016, **170A**:435–440.

180. Kawabata Galbraith K, Kengaku M: **Multiple roles of the actin and microtubule-regulating formins in the developing brain**. *Neurosci Res* 2019, **138**:59–69.

181. Thumkeo D, Shinohara R, Watanabe K, Takebayashi H, Toyoda Y, Tohyama K, Ishizaki T, Furuyashiki T, Narumiya S: **Deficiency of mDia, an actin nucleator, disrupts integrity of neuroepithelium and causes periventricular dysplasia**. *PLoS One* 2011, **6**.

182. Shinohara R, Thumkeo D, Kamijo H, Kaneko N, Sawamoto K, Watanabe K, Takebayashi H, Kiyonari H, Ishizaki T, Furuyashiki T, et al.: **A role for mDia, a Rho-regulated actin nucleator, in tangential migration of interneuron precursors**. *Nat Neurosci* 2012, **15**:373–380.

183. Toyoda Y, Shinohara R, Thumkeo D, Kamijo H, Nishimaru H, Hioki H, Kaneko T, Ishizaki T, Furuyashiki T, Narumiya S: **EphA4-dependent axon retraction and midline localization of Ephrin-B3 are disrupted in the spinal cord of mice lacking mDia1 and mDia3 in combination**. *Genes Cells* 2013, **18**:873–885.

184. Arakawa Y, Bito H, Furuyashiki T, Tsuji T, Takemoto-Kimura S, Kimura K, Nozaki K, Hashimoto N, Narumiya S: **Control of axon elongation via an SDF-1alpha/Rho/mDia pathway in cultured cerebellar granule neurons**. *J Cell Biol* 2003, **161**:381–391.

185. Ohshima Y, Kubo T, Koyama R, Ueno M, Nakagawa M, Yamashita T: **Regulation of axonal elongation and pathfinding from the entorhinal cortex to the dentate gyrus in the hippocampus by the chemokine stromal cell-derived factor 1 alpha**. *J Neurosci* 2008, **28**:8344–8353.

186. Zhang W, Ciorraga M, Mendez P, Retana D, Boumedine-Guignon N, Achón B, Russier M, Debanne D, Garrido JJ: **Formin Activity and mDia1 Contribute to Maintain Axon Initial Segment Composition and Structure**. *Mol Neurobiol* 2021, **58**:6153.

187. Hong EH, Kim JY, Kim JH, Lim DS, Kim M, Kim JY: **BIG2-ARF1-RhoA-mDia1 Signaling Regulates Dendritic Golgi Polarization in Hippocampal Neurons**. *Mol Neurobiol* 2018, **55**:7701–7716.

188. Zilberman Y, Alieva NO, Miserey-Lenkei S, Lichtenstein A, Kam Z, Sabanay H, Bershadsky A: **Involvement of the Rho-mDia1 pathway in the regulation of Golgi complex architecture and dynamics**. *Mol Biol Cell* 2011, **22**:2900–2911.

189. Qu X, Yuan FN, Corona C, Pasini S, Pero ME, Gundersen GG, Shelanski ML, Bartolini F: **Stabilization of dynamic microtubules by mDia1 drives Tau-dependent Aβ 1-42 synaptotoxicity**. *J Cell Biol* 2017, **216**:3161–3178.

190. Peng J, Kitchen SM, West RA, Sigler R, Eisenmann KM, Alberts AS: **Myeloproliferative defects following targeting of the Drf1 gene encoding the mammalian diaphanous related formin mDia1**. *Cancer Res* 2007, **67**:7565–7571.

191. Prager-Khoutorsky M, Bourque CW: **Osmosensation in vasopressin neurons: changing actin density to optimize function**. *Trends Neurosci* 2010, **33**:76–83.

192. Pilpel Y, Segal M: **Activation of PKC induces rapid morphological plasticity in dendrites of hippocampal neurons via Rac and Rho-dependent mechanisms**. *Eur J Neurosci* 2004, **19**:3151–3164.

193. Kjøller L, Hall A: **Signaling to Rho GTPases**. *Exp Cell Res* 1999, **253**:166–179.

194. Sah VP, Seasholtz TM, Sagi SA, Brown JH: **The role of Rho in G protein-coupled receptor signal transduction**. *Annu Rev Pharmacol Toxicol* 2000, **40**:459–489.

195. Sternweis PC, Carter AM, Chen Z, Danesh SM, Hsiung YF, Singer WD: **Regulation of Rho guanine nucleotide exchange factors by G proteins**. *Adv Protein Chem* 2007, **74**:189–228.

196. Higuchi S, Ohtsu H, Suzuki H, Shirai H, Frank GD, Eguchi S: **Angiotensin II signal transduction through the AT1 receptor: novel insights into mechanisms and pathophysiology**. *Clin Sci (Lond)* 2007, **112**:417–428.

197. Kuwahara M, Kuwahara M: **Involvement of Rho and tyrosine kinase in angiotensin II-induced actin reorganization in mesothelial cells**. *Eur J Pharmacol* 2002, **436**:15–21.

198. Aoki H, Izumo S, Sadoshima J: **Angiotensin II activates RhoA in cardiac myocytes: a critical role of RhoA in angiotensin II-induced premyofibril formation**. *Circ Res* 1998, **82**:666–676.

199. Barnes WG, Reiter E, Violin JD, Ren XR, Milligan G, Lefkowitz RJ: **beta-Arrestin 1 and Galphaq/11 coordinately activate RhoA and stress fiber formation following receptor stimulation**. *J Biol Chem* 2005, **280**:8041–8050.

200. Wirth A, Benyó Z, Lukasova M, Leutgeb B, Wettschureck N, Gorbey S, Orsy P, Horváth B, Maser-Gluth C, Greiner E, et al.: **G12-G13-LARG-mediated signaling in vascular smooth muscle is required for salt-induced hypertension**. *Nat Med* 2008, **14**:64–68.

201. Ying Z, Jin L, Dorrance AM, Clinton Webb R: **Increaseed expression of mRNA for regulator of G protein signaling domain-containing Rho guanine nucleotide exchange factors in aorta from stroke-prone spontaneously hypertensive rats**. *Am J Hypertens* 2004, **17**:981–985.

202. Ying Z, Jin L, Palmer T, Webb RC: **Angiotensin II up-regulates the leukemia-associated Rho guanine nucleotide exchange factor (RhoGEF), a regulator of G protein signaling domain-containing RhoGEF, in vascular smooth muscle cells**. *Mol Pharmacol* 2006, **69**:932–940.

203. Porchia F, Papucci M, Gargini C, Asta A, De Marco G, Agretti P, Tonacchera M, Mazzoni MR: **Endothelin-1 up-regulates p115RhoGEF in embryonic rat cardiomyocytes during the hypertrophic response**. *J Recept Signal Transduct Res* 2008, **28**:265–283.

204. Ajayi AF, Akhigbe RE: **Staging of the estrous cycle and induction of estrus in experimental rodents: an update**. *Fertil Res Pract* 2020, **6**.

205. Prager-Khoutorsky M, Bourque CW: **Anatomical organization of the rat organum vasculosum laminae terminalis**. *Am J Physiol Regul Integr Comp Physiol* 2015,

309:R324–R337.

206. Lee LC, Sasaki S, Inoue A, Fukuyama M, Nakamura Y, Oguro M, Kawasaki S, Hayashi J, Takeda K, Yoshimura M, et al.: **Salt increases blood pressure with biphasic changes in hypothalamic responsiveness in rats**. *J Cardiovasc Pharmacol* 1988, **12**:179–185.

207. Velasquez MT, Alexander N: **Blood pressure and sodium excretion in the sinoaortic denervated rat during chronic high and low sodium intake and acute sodium loading**. *Clin Exp Hypertens A* 1982, **4**:499–519.

208. Osborn JW, Hornfeldt BJ: **Arterial baroreceptor denervation impairs long-term regulation of arterial pressure during dietary salt loading**. *Am J Physiol* 1998, **275**.

209. Bardgett ME, Holbein WW, Herrera-Rosales M, Toney GM: **Ang II-salt hypertension depends on neuronal activity in the hypothalamic paraventricular nucleus but not on local actions of tumor necrosis factor-α**. *Hypertens (Dallas, Tex 1979)* 2014, **63**:527–534.

210. Iyer A, Chan V, Brown L: **The DOCA-Salt Hypertensive Rat as a Model of Cardiovascular Oxidative and Inflammatory Stress**. *Curr Cardiol Rev* 2010, **6**:291.

211. Crestani S, Webb RC, Da Silva-Santos JE: **High-Salt Intake Augments the Activity of the RhoA/ROCK Pathway and Reduces Intracellular Calcium in Arteries From Rats**. *Am J Hypertens* 2017, **30**:389.

212. Tolins JP, Shultz PJ: **Endogenous nitric oxide synthesis determines sensitivity to the pressor effect of salt**. *Kidney Int* 1994, **46**:230–236.

213. Crestani S, Gasparotto Júnior A, Marques MCA, Sullivan JC, Webb RC, Da Silva-Santos JE: **Enhanced angiotensin-converting enzyme activity and systemic reactivity to angiotensin II in normotensive rats exposed to a high-sodium diet**. *Vascul Pharmacol* 2014, **60**:67–74.

214. Gürtler A, Kunz N, Gomolka M, Hornhardt S, Friedl AA, McDonald K, Kohn JE, Posch A: **Stain-Free technology as a normalization tool in Western blot analysis**. *Anal Biochem* 2013, **433**:105–111.

215. Kramár EA, Chen LY, Brandon NJ, Rex CS, Liu F, Gall CM, Lynch G: **Cytoskeletal changes underlie estrogen's acute effects on synaptic transmission and plasticity**. *J Neurosci* 2009, **29**:12982–12993.

216. Riveline D, Zamir E, Balaban NQ, Schwarz US, Ishizaki T, Narumiya S, Kam Z, Geiger B, Bershadsky AD: **Focal contacts as mechanosensors: Externally applied local mechanical force induces growth of focal contacts by an mDia1-dependent and ROCK-independent mechanism**. *J Cell Biol* 2001, **153**:1175–1185.

217. Hicks AI, Barad Z, Sobrero A, Lean G, Jacob-Tomas S, Yang J, Choe KY, Prager-Khoutorsky M: **Effects of salt loading on the organisation of microtubules in rat magnocellular vasopressin neurones**. *J Neuroendocrinol* 2020, **32**:1–9.

218. Sen S, Tarazi RC, Khairallah PA, Bumpus FM: **Cardiac Hypertrophy in Spontaneously Hypertensive Rats**. *Circ Res* 1974, **35**:775–781.

219. Rapp JP: **Dahl Salt-Susceptible and Salt-Resistant Rats A Review**. [date unknown],

220. Rhodes CH, Morriell JI, Pfaff DW: **Immunohistochemical analysis of magnocellular elements in rat hypothalamus: Distribution and numbers of cells containing neurophysin, oxytocin, and vasopressin**. *J Comp Neurol* 1981, **198**:45–64.

221. Levi DI, Wyrosdic JC, Hicks A, Andrade MA, Toney GM, Prager-khoutorsky M, Bourque CW, Levi DI, Wyrosdic JC, Hicks A, et al.: **Article High dietary salt amplifies osmoresponsiveness in vasopressin-releasing neurons ll High dietary salt amplifies osmoresponsiveness in vasopressin-releasing neurons**. *CellReports* 2021, **34**:108866.

222. Li F, Higgs HN: **The Mouse Formin mDia1 Is a Potent Actin Nucleation Factor Regulated by Autoinhibition**. *Curr Biol* 2003, **13**:1335–1340.

223. Watanabe N, Kato T, Fujita A, Ishizaki T, Narumiya S: **Cooperation between mDia1 and ROCK in Rho-induced actin reorganization**. *Nat Cell Biol 1999 13* 1999, **1**:136–143.

224. Sajib MS, Zahra FT, Akwii RG, Mikelis CM: **Identification of Rho GEF and RhoA Activation by Pull-Down Assays**. *Methods Mol Biol* 2021, **2193**:97–109.

225. Rizvi SA, Neidt EM, Cui J, Feiger Z, Skau CT, Margaret L, Kozmin SA, Kovar DR: **Identification and Characterization of a Small Molecule Inhibitor of Formin-Mediated Actin Assembly**. 2010, **16**:1158–1168.

226. Baell JB: **Observations on screening-based research and some concerning trends in the literature**. *Future Med Chem* 2010, **2**:1529–1546.

227. Isogai T, Kammen R Van Der, Innocenti M: **SMIFH2 has effects on Formins and p53 that perturb the cell cytoskeleton**. 2015, doi:10.1038/srep09802.

228. Nishimura Y, Shi S, Zhang F, Liu R, Takagi Y, Bershadsky AD, Viasnoff V, Sellers JR: **The Formin Inhibitor, SMIFH2, Inhibits Members of the Myosin Superfamily**. 2020,

229. Lecorgne H, Tudosie AM, Lavik K, Su R, Becker KN, Moore S, Walia Y, Wisner A, Koehler D, Alberts AS, et al.: **Differential Toxicity of mDia Formin-Directed Functional Agonists and Antagonists in Developing Zebrafish**. 2018, **9**:1–10.

230. Janson J, Andersson G, Bergquist L, Eriksson M, Folgering JHA: **Impact of chemical modification of sulfamidase on distribution to brain interstitial fluid and to CSF after an intravenous administration in awake, freely-moving rats**. *Mol Genet Metab Reports* 2020, **22**:100554.

231. Alberts AS, Bouquin N, Johnston LH, Treisman R: **Analysis of RhoA-binding Proteins Reveals an Interaction Domain Conserved in Heterotrimeric G Protein β Subunits and the Yeast Response Regulator Protein Skn7 ***. *J Biol Chem* 1998, **273**:8616–8622.

232. Higashi T, Ikeda T, Shirakawa R, Kondo H, Kawato M, Horiguchi M, Okuda T, Okawa K, Fukai S, Nureki O, et al.: **Biochemical Characterization of the Rho GTPase-regulated Actin Assembly by Diaphanous-related Formins, mDia1 and Daam1, in Platelets ***. *J Biol Chem* 2008, **283**:8746–8755.

233. Habas R, Kato Y, He X: **Wnt/Frizzled activation of Rho regulates vertebrate gastrulation and requires a novel formin homology protein Daam1**. *Cell* 2001, **107**:843–854.

234. Nakamura F, Ohshima T, Goshima Y: **Collapsin Response Mediator Proteins: Their Biological Functions and Pathophysiology in Neuronal Development and Regeneration**. *Front Cell Neurosci* 2020, **14**:1–13.

235. Khazaei MR, Girouard MP, Alchini R, Tone SO, Shimada T, Bechstedt S, Cowan M, Guillet D, Wiseman PW, Brouhard G, et al.: **Collapsin response mediator protein 4 regulates growth cone dynamics through the actin and microtubule cytoskeleton**. *J Biol Chem* 2014, **289**:30133–30143.